Early View publication on www.wileyonlinelibrary.com
(issue and page numbers not yet assigned;
citable using Digital Object Identifier – DOI)

LASER & PHOTONICS REVIEWS

Laser Photonics Rev., 1–22 (2011) / **DOI** 10.1002/lpor.201000031

Abstract This paper provides an overview of the rather new field concerning the applications of femtosecond laser microstructuring of glass to optofluidics. Femtosecond lasers have recently emerged as a powerful microfabrication tool due to their unique characteristics. On the one hand, they enable to induce a permanent refractive index increase, in a micrometer-sized volume of the material, allowing single-step, three-dimensional fabrication of optical waveguides. On the other hand, femtosecond-laser irradiation of fused silica followed by chemical etching enables the manufacturing of directly buried microfluidic channels. This opens the intriguing possibility of using a single laser system for the fabrication and three-dimensional integration of optofluidic devices. This paper will review the state of the art of femtosecond laser fabrication of optical waveguides and microfluidic channels, as well as their integration for high sensitivity detection of biomolecules and for cell manipulation.

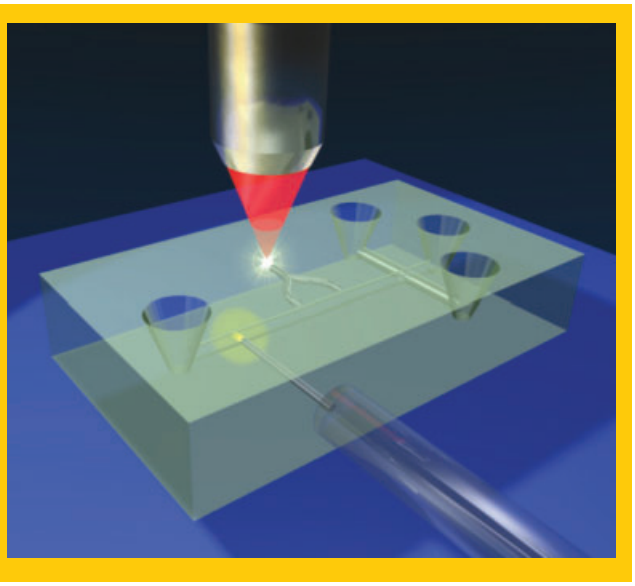

Femtosecond laser microstructuring: an enabling tool for optofluidic lab-on-chips

Roberto Osellame[1], Hugo J. W. M. Hoekstra[2], Giulio Cerullo[1,*], and Markus Pollnau[2]

1. Introduction

Lab-on-chips (LOCs) are microsystems aiming at the miniaturization onto a single substrate of several functionalities that typically would require an entire biological laboratory [1–4]. LOCs use networks of microfluidic channels to transport, mix, separate, react and analyze very small volumes (micro- to nanoliters) of biological samples. The main advantages of the LOC approach are high sensitivity, speed of analysis, low sample and reagent consumption, and measurement automation and standardization. Applications of LOCs range from biochemical research (genomics, proteomics and cellomics), to chemical synthesis and drug development [5], high-throughput medical and biochemical analysis [6], environmental monitoring and detection of chemical and biological threats. Thanks to the miniaturization and integration afforded by LOCs, the life sciences are undergoing a revolution similar to that triggered by integrated microelectronic systems, which gave birth to the Information Society. Comprehensive reviews of the fundamentals and potentials of LOC technology can be found in [7–9].

Several substrate materials are used for LOC fabrication, including silicon, glass and polymers. Although polymers have the advantages of a very low cost and of the simplicity of microchannel fabrication by molding or embossing, glass is still the material of choice for many applications [10] due to the following benefits: it is chemically inert, stable in time, hydrophilic, nonporous, optically clear, and it easily supports electro-osmotic flow. In particular, the choice of fused silica as the substrate material adds to the previous advantages a very high optical transparency, down to the UV range, and a very low background fluorescence. In addition, well established microfabrication processes, based on photolithography and wet/dry etching, are available for this glass [11].

While many different fluidic functions have already been implemented on LOCs, a key unsolved problem is the development of an integrated on-chip detection system [12]. The main reason for this is that, as the size of the microfluidic systems shrinks more and more, also the detection volumes become smaller and smaller, decreasing the number of interrogated molecules and calling for a very high sensitivity. Electrochemical and optical are the two most widespread detection schemes for LOCs. Optical measurements are superior both in terms of flexibility and sensitivity; in particular, laser-induced fluorescence (LIF) detection of labelled molecules, being a background-free technique, allows the measurement of very low analyte concentrations. In addi-

[1] Istituto di Fotonica e Nanotecnologie (IFN)-CNR, Dipartimento di Fisica-Politecnico di Milano, Piazza Leonardo da Vinci 32, 20133 Milan, Italy [2] Integrated Optical Microsystems Group, MESA+ Institute for Nanotechnology, University of Twente, P. O. Box 217, 7500 AE Enschede, The Netherlands
[*] Corresponding author: e-mail: giulio.cerullo@fisi.polimi.it

tion to detection, light can be used for different purposes in LOCs such as steering and trapping of cells, nanoparticles and molecules [13].

In traditional optical setups used in conjunction with LOCs, both excitation and detection are performed using bulk optical equipment, such as mirrors, lenses and microscope objectives, to focus the excitation light into a tiny measurement volume and to collect the resulting fluorescence [1, 2]. Such schemes require accurate mechanical alignment of the optical components to the microfluidic channels and allow only a limited number of excitation/detection configurations, typically in a single point confocal arrangement. The coupling of a miniaturized LOC system with a massive benchtop instrument, such as an optical microscope, frustrates many of the LOC advantages, in particular it strongly limits device portability and prevents on-field or point-of-care applications. Much of the commercial success of the LOC concept will therefore critically depend on the ability to successfully integrate optical excitation/detection schemes.

Several efforts have been performed in order to fabricate on-chip micro-optical components to perform optical detection [14–16]. The most widely used components are optical waveguides, which allow to confine and transport light in the chip directing it to a small volume of the microfluidic channel and collecting the transmitted/emitted light. However, the integration of optical waveguides or more complex photonic components with microfluidic channels is not a straightforward process. In fact it requires a local modification of the refractive index of the substrate, which means adding further lithographic steps, thus complicating the fabrication process of the chip. Depending on the substrate of choice, different methods can be used. Approaches reported in the literature include waveguide fabrication by silica on silicon [14–17], ion exchange in soda-lime glasses [18, 19], photolithography in polymers [20, 21] and liquid-core waveguides [22–25]. All these methods suffer, when applied to LOCs, from several limitations: (i) they are inherently planar techniques, i. e. they are able to define optical guiding structures only in two dimensions, close to the sample surface; (ii) they are multistep methods, involving multiple masking with critical alignments; (iii) they require cleanroom environment, and (iv) they typically create uneven surfaces which make sealing of the microfluidic channels problematic. Such problems have so far strongly limited the integration of optical waveguides with microfluidic chips.

Recently, femtosecond laser writing [26] has emerged as a novel powerful approach for the integration of optical waveguides into LOCs. This technique presents some unique advantages which overcome the previously described limitations: (i) it is a direct maskless fabrication technique, i. e. in a single step one can create optical waveguides or more complicated photonic devices (splitters, interferometers, etc.) by simply moving the sample with respect to the laser focus, avoiding complex clean room facilities; (ii) it is a three-dimensional (3D) technique, since it allows one to define waveguides at arbitrary depths inside the glass [27]. The first feature allows to add waveguides, by simple post-processing, inside LOCs that have been fabricated by standard technologies, enabling a straightforward upgrade of chips that have already been optimized for microfluidic functionality. The second feature gives a much greater freedom in the device design, allowing novel and more compact geometries and unprecedented functionalities exploiting the 3D architecture. In addition to waveguide writing, femtosecond lasers also offer the possibility of direct fabrication of microfluidic channels in fused silica, by the technique known as Femtosecond Laser Irradiation followed by Chemical Etching (FLICE) [28]. The FLICE technique consists of two steps: 1) permanent sample modification following nonlinear absorption of focused femtosecond laser pulses; 2) etching of the laser modified zone by a hydrofluoric acid (HF) solution in water. Femtosecond laser irradiation, by a mechanism discussed in Sect. 3, enhances the etching rate by up to two orders of magnitude, enabling the manufacturing of channels with high aspect ratio.

The FLICE technique has to compete with conventional approaches for the fabrication of microfluidic channels, borrowed from semiconductor processing, such as wet chemical etching and deep reactive ion etching [11]. These techniques require a clean room facility and create a 2D open channel network at the surface of the sample, that needs to be sealed by a glass slab to obtain the microfluidic channels; moreover, 3D structures are very complex to produce by these methods, since they would require a multilayer processing. The FLICE approach, although it produces channels that are presently limited in length to a few millimeters, has some distinct advantages: (i) it avoids photolithography and clean rooms; (ii) it creates directly buried channels which do not require sealing with a cover glass; (iii) it naturally produces channels with a circular cross section, which are not easily obtained by other techniques; (iv) it allows straightforward fabrication of channels with 3D geometries.

The possibility of combining optical waveguide writing with the FLICE technique provides the exciting opportunity of using a single platform, based on femtosecond laser microstructuring, for fabricating microfluidic devices with integrated optical sensing. It should also be noted that the integration, on the same substrate, of optical and microfluidic components has far-reaching scientific and technological implications, that go beyond the specific application of sensing in LOCs. To define this new field of research, the terms "optofluidics" has been recently introduced in the scientific literature [29,30]. Optofluidics exploits the synergy of optics and fluidics for the realization of completely new functionalities, such as optical elements whose properties can be tuned through fluid replacement or modification, resulting in reconfigurable and adaptive microphotonic devices [31].

This paper provides an overview of the rather new field concerning the applications of femtosecond laser microstructuring to optofluidics. It first aims at describing the research performed so far, with particular emphasis on the results by the authors. It also has the ambition to bridge a gap between different communities, at the same time proposing an exciting application field to the researchers working on femtosecond microfabrication and making the final users of micro/optofluidic devices aware of new technological opportunities. The paper is organized as follows: in Sect. 2

we review the fundamental physical mechanisms underlying femtosecond laser optical waveguide writing and discuss the typical waveguide properties in glass; in Sect. 3 we introduce the FLICE technique, its performances and limitations, and discuss the integration of optical waveguides and microfluidic channels, both fabricated by femtosecond technology. In Sect. 4 we present examples of optofluidic devices, which are partially or completely fabricated by femtosecond laser technology, for detection and/or manipulation of biomolecules and cells. Finally in Sect. 5 we draw the conclusions and discuss further developments.

2. Femtosecond laser waveguide writing

2.1. Fundamental physical mechanisms

In order to understand the physical phenomena underlying optical waveguide writing by femtosecond laser pulses, it is necessary to first briefly analyze the absorption processes of intense laser pulses by transparent dielectric materials. Since these materials have an energy gap E_g greater than the laser photon energy $h\nu$, there is no linear absorption through interband transitions from valence to conduction band. At high intensities, however, absorption can take place through nonlinear phenomena, such as multiphoton, tunneling and avalanche ionization.

Multiphoton ionization (see Fig. 1a) involves the simultaneous absorption of m photons, where m is the minimum integer such that $mh\nu > E_g$. Tunnelling ionization (see Fig. 1b) occurs when the very high electric field of the laser pulse lowers the Coulomb potential energy barrier and enables an electron to tunnel from the valence to the conduction band. At high intensities the multiphoton and tunnelling ionization processes compete [32] and can be distinguished by the so-called Keldysh parameter, $\gamma = \omega(2m*E_g)^{1/2}/e\mathscr{E}$, where $m*$ and e are the effective mass and charge of the electron and $\mathscr{E}$ is the amplitude of the electric field oscillating at frequency ω. If γ is much smaller (greater) than 1.5, tunneling (multiphoton) ionization dominates. For $\gamma \sim 1.5$, photoionization is a combination of tunneling and multiphoton ionization. For waveguide fabrication in dielectrics, typical laser and material properties result in $\gamma \sim 1$, so that nonlinear ionization is a combination of both processes [32].

To understand the avalanche ionization process (Fig. 1c), let us suppose that an electron is free at the bottom of the conduction band of the material; if exposed to an intense light field, it is accelerated and acquires kinetic energy. When its total energy exceeds the conduction band minimum by more than the bandgap energy, it can ionize another electron from the valence band, resulting in two electrons near the conduction band minimum. These electrons can be in turn accelerated by the electric field, causing an avalanche in which the free electron density grows exponentially; for sufficiently high densities, the dielectric becomes strongly absorbing.

Let us now compare the nonlinear absorption mechanisms with "long" (multiple picoseconds to nanosecond duration) and "short" (sub-picosecond duration) laser pulses [34]. If the dielectric is illuminated by a long pulse, the peak intensity is too low to allow multiphoton or tunnelling ionization, even if the total pulse energy might be rather high. The only possible absorption mechanism is avalanche ionization starting from an initial "seed" of free electrons in the conduction band which, being the material an insulator, are due to impurities and dislocations within the focal volume of the laser pulse. Since their number is subject to large fluctuations, the absorption process is erratic and poorly reproducible. With short laser pulses, on the other hand, the peak intensities are much higher and multiphoton/tunnelling ionization becomes significant. When the intensity exceeds a given threshold, some free electrons are generated in the focal volume by these mechanisms. These electrons act as a *seed*, generated in a fully deterministic fashion, for the avalanche ionization process, which increases the number of free electrons in the dielectric until the plasma frequency approaches the laser frequency, at which point the material becomes strongly absorbing. This has been clearly demonstrated by Rayner et al., who showed that at intensities of 8×10^{14} W/cm^2 nearly 90% of the energy of a 50-fs 800-nm laser pulse is absorbed by a pyrex substrate [35]. In addition, with short excitation pulses, the free electron plasma is formed on a timescale much shorter than that necessary for energy transfer to the lattice (typically of a few picoseconds). It is therefore clear that only high intensity femtosecond pulses allow to depose energy in a controlled and reproducible fashion in a small volume inside the bulk of a transparent material.

Following nonlinear absorption and energy transfer to the lattice, permanent material modification can occur if the deposited energy exceeds a given threshold. The resulting morphological changes depend on the exposure parameters (energy, pulse duration, repetition rate, wavelength, ...)

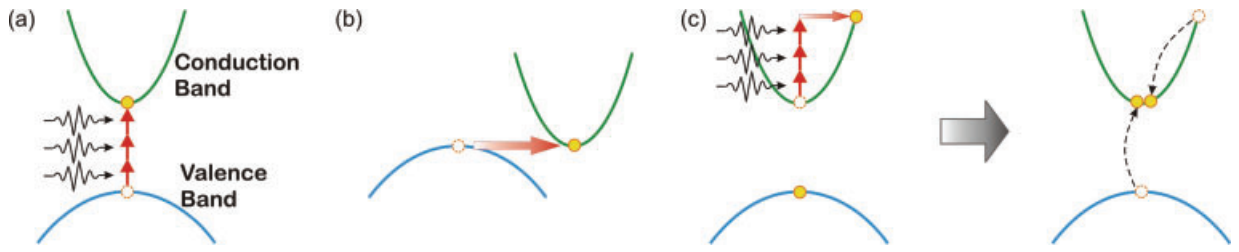

Figure 1 (online color at: www.lpr-journal.org) Schematics of the nonlinear absorption processes induced by femtosecond laser pulses in transparent materials: (a) multiphoton absorption, (b) tunnelling ionization and (c) avalanche ionization [33].

and on the material properties (bandgap, thermal conductivity, ...). Broadly speaking, they can be classified into three categories, in order of increasing laser fluence [36–38]:

a) for a fluence just above the permanent modification threshold, a smooth modification is achieved, resulting mainly in positive/negative refractive index changes;
b) for higher fluence, sub-wavelength nanogratings [37] are formed (so far only observed in fused silica glass), oriented perpendicularly to the writing laser polarization and with period $\approx \lambda/2n$, where λ is the laser wavelength and n the refractive index of the substrate;
c) for even higher fluence, a disruptive modification is obtained, with the creation of voids and microexplosions [39, 40].

Regime (a) is the one typically used for waveguide fabrication, while regime (b) is the one employed in the first step of the FLICE technique for microchannel production, and will be described in detail in Sect. 3. Regime (c) can be used for direct laser ablation and it will not be further considered in this paper.

The physical mechanisms underlying permanent refractive index changes in glasses are not yet fully understood. Several phenomena have been proposed to explain these changes, none of which seems to be fully general. A first possible mechanism is colour center formation: the femtosecond irradiation produces in the material a sufficient number of color centers which, while absorbing in the UV, modify by the Kramers-Kroenig mechanism the refractive index at the wavelengths of interest [41]. This is the mechanism for the index change produced by deep-UV excitation of the Ge-doped silica fibers used in fiber Bragg gratings and evidence has been brought for its contribution to refractive index changes in femtosecond laser written waveguides [42]. An alternative mechanism is thermally induced material densification: energy deposited by the laser melts the material in the focal volume, and the subsequent rapid resolidification dynamics lead to density (and therefore refractive index) variations [43]. Some glass types, such as fused silica, increase their density at higher temperatures; if they are rapidly cooled (quenched), the higher density (and therefore higher refractive index) structural arrangement is "frozen in". Another possible mechanism responsible for waveguide formation is non-uniform cooling. After irradiation, the material melts out to a radius where the temperature equals the melting temperature of the glass. Molten material just inside this maximum radius then quickly quenches and solidifies into a lower-density structural arrangement of the glass. This quenching continues radially inward as the glass continues to cool. Because there is no free surface that can expand to take up the extra volume occupied by the less dense glass formed by this quenching, the material near the focal region is put under pressure. As a result of this pressure, the material near the focal region solidifies into a higher density phase, leading to the higher refractive index at the core of the structures. Finally, another possible mechanism is direct structural change induced by the femtosecond laser pulses, i. e. rearrangement of the network of chemical bonds in the glass matrix leading to a density increase [44]. In practical cases, all the three mechanisms discussed above may play a role in refractive index change and it is difficult to disentangle their relative contributions.

Finally it is worth noting that in crystalline materials femtosecond laser irradiation generally produces a decrease in refractive index; this can be easily understood by considering that in a crystal the atoms are in the closest possible arrangement and that any change in the lattice order will lead to a lower density. Optical waveguides can nevertheless be created on the sides of the modified region, where stresses induce a refractive index increase [45, 46].

2.2. Methods for femtosecond waveguide writing

Nonlinear absorption in glasses takes place for intensities around $1–5 \times 10^{13}$ W/cm^2 that, for a pulse duration of 100 fs, correspond to fluences of 1–5 J/cm^2. The pulse energy required to achieve such fluences depends on the focusing conditions: For "mild" focusing (1–3-μm beam waist), it is at the level of a few μJs, while for extremely tight focusing, of the order of a half-wavelength (diffraction limited), it can be reduced to a few tens of nJs.

Two different regimes of femtosecond waveguide writing can be distinguished, depending on whether the pulse period is longer or shorter than the time required for heat to diffuse away from the focal volume: the "low-frequency" regime, in which material modification is produced by the individual pulses, and the "high-frequency" regime, in which cumulative effects take place. Since the heat diffusion time out of the absorption volume in glass can be estimated at ≈ 1 μs, the transition between the two regimes takes place at frequencies around 1 MHz. Low-frequency systems typically use regeneratively amplified Ti:sapphire lasers (1–200 kHz repetition rate) [26, 47, 48]. The high-frequency regime was initially accessed using Ti:sapphire oscillators with the cavity length stretched by a telescope or a multipass cell (5–20-MHz repetition rate) [49–52]. Recently, Yb-based bulk or fiber lasers, working at repetition rates from a few hundreds kHz to a few MHz, have become increasingly widespread and have provided the best fabrication results [53–56].

Two different writing geometries are possible, longitudinal and transverse, in which the sample is translated, respectively, along and perpendicularly to the beam propagation direction. In the longitudinal geometry, the waveguides are intrinsically symmetric, and their transverse size is determined by the focal spot size, making it possible to achieve fairly large diameters; however, the waveguide length is limited by the focal length of the focusing objective, and their quality is degraded by spherical aberrations as the depth of the focus inside the glass sample increases. The transverse geometry provides a much greater flexibility and allows one to write waveguides or waveguide structures of arbitrary length and geometry; it has, however, the disadvantage of producing a strong asymmetry in the waveguide cross section [57]. This asymmetry can be explained as follows: perpendicularly to the beam propagation direction, the waveguide size is given approximately by the beam focal diameter $2w_0$, while along the propagation direction, it is

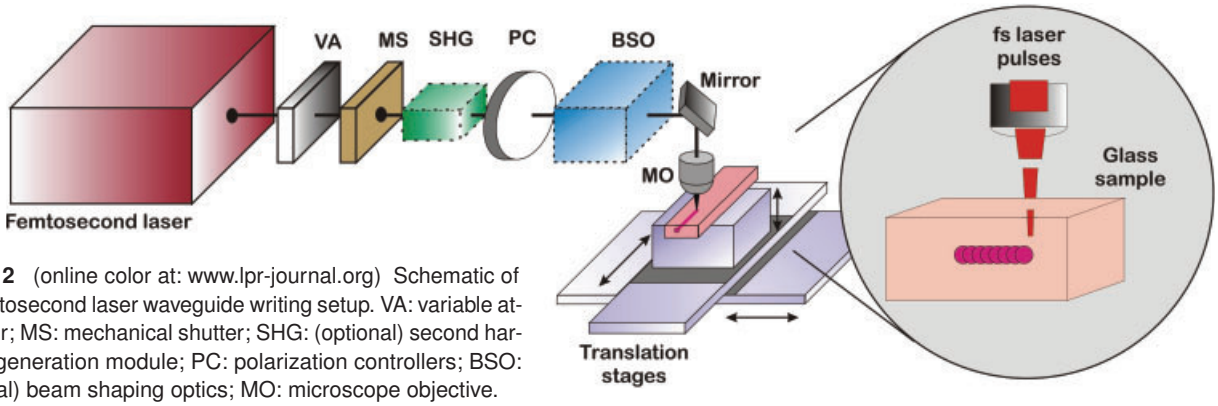

Figure 2 (online color at: www.lpr-journal.org) Schematic of the femtosecond laser waveguide writing setup. VA: variable attenuator; MS: mechanical shutter; SHG: (optional) second harmonic generation module; PC: polarization controllers; BSO: (optional) beam shaping optics; MO: microscope objective.

given by the confocal parameter $b = 2\,\pi w_0^2/\lambda$. For focused diameters of the order of a few micrometers, this results in a large difference in waveguide sizes in the two directions. This problem can be overcome [58, 59] by introducing a focusing geometry in which the femtosecond writing beam is astigmatically shaped by changing both the spot sizes in the tangential and sagittal planes and the relative positions of the beam waists. This shaping allows one to modify the interaction volume in such a way that the waveguide cross section is circular and with arbitrary size. The astigmatic beam shaping can be easily obtained by a cylindrical telescope before the focusing objective. The same effect of focal volume shaping in order to decrease the confocal parameter can also be obtained by the use of a slit, oriented parallel to the laser scanning direction, before the focusing lens [60]. This arrangement also creates waveguides with symmetric cross section, but has the disadvantage of wasting most of the laser power impinging on the slit. Alternative approaches for controlling the waveguide cross section are multiscan writing [61] and spatial beam shaping with a deformable mirror [62]. The asymmetry problem is naturally overcome in the high frequency writing regime, since isotropic heat diffusion leads to a symmetric waveguide cross section [63].

Figure 2 shows a scheme of a typical system used for femtosecond laser waveguide writing. The same system is also used for the irradiation step of the FLICE process. Pulses from the femtosecond laser pass, in sequence, a variable attenuator, a mechanical shutter, an optional second harmonic generation stage, a polarization controller and optional beam shaping optics; the pulses are then focussed (typically by a microscope objective) inside the glass substrate. The sample is moved by a computer-controlled 3D translation stage, which allows to inscribe the desired structure. The system is remarkably simple and flexible.

2.3. Waveguide properties in fused silica

Optical waveguides and integrated photonic devices have been written in a variety of glasses and crystalline materials. In the following we will focus on the fabrication and optical properties of waveguides in fused silica, since this is the most interesting material for optofluidic applications.

A first waveguide writing approach used a low repetition rate laser system. The results were achieved with

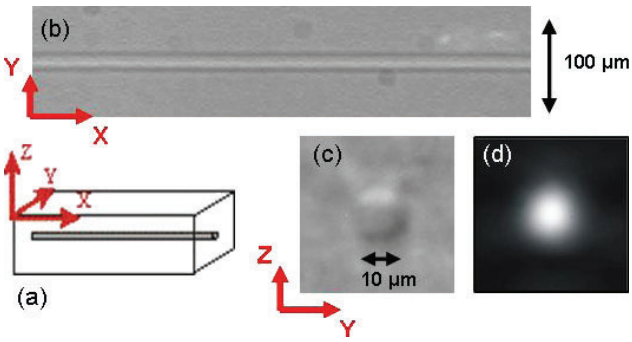

Figure 3 (online color at: www.lpr-journal.org) Optical waveguides in fused silica written at low repetition rate. (a) Schematic of a glass chip with an optical waveguide; (b) microscope image of the waveguide from the top; (c) microscope image of the waveguide cross-section; (d) near-field of the guided mode at 543 nm wavelength.

an amplified Ti:sapphire laser (800-nm wavelength, 1-kHz repetition rate, ≈ 100-fs pulsewidth) using 4-µJ pulse energy, mild focusing (20× objective, 0.3 NA) and 20-µm/s translation speed [64]. The astigmatic beam shaping technique [58, 59] was employed to obtain circular waveguide cross section. Figure 3 shows a top view (Fig. 3b) and an end view (Fig. 3c) of such a waveguide, with a diameter of about 10 µm. Note that the material modification is strictly limited to the focal volume of the writing beam; this is quite important for optical sensing in LOCs where the control of the waveguide position with respect to the microfluidic channels is necessary. The refractive index contrast is of the order of $\Delta n = 1 \times 10^{-3}$, resulting in single-mode operation throughout the visible range (see Fig. 3d). Propagation losses at 543 nm, measured using the cut-back technique, were found to be 0.9 dB/cm. This value is very promising as compared to those obtained at similar wavelengths in other kinds of waveguides integrated on LOCs and fabricated with SU-8 polymer (2.5 dB/cm) [21] and with SiON technology (1 dB/cm) [17].

Such fabrication parameters are ideal for straight waveguides to achieve selective spatial excitation of the contents of a microfluidic channel (see Sect. 4.1). On the other hand, the refractive index contrast is not sufficient for fabricating curved waveguides, which are required in several photonic

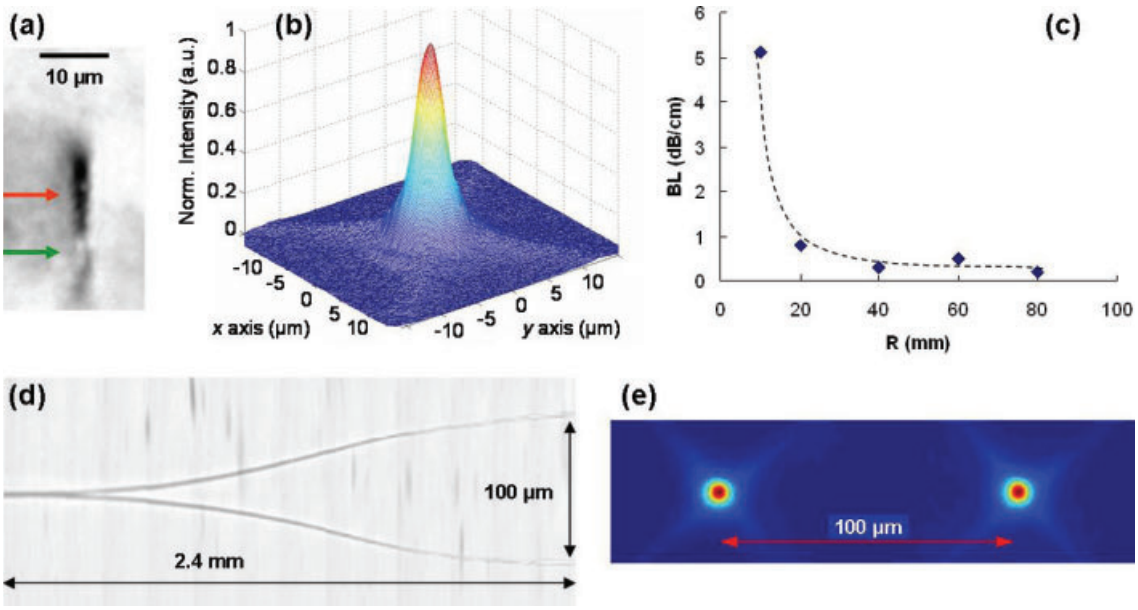

Figure 4 (online color at: www.lpr-journal.org) (a) Microscope image of the cross-section of a waveguide written at high repetition rate – red arrow points to the damaged region, green arrow points to the waveguiding portion; (b) near field intensity of the guided mode; (c) characterization of the waveguide bending losses (BL) as a function of the curvature radius R; (d) microscope image of a Y-junction optical splitter (note that the horizontal and vertical scales are different); (e) near field intensity of the optical splitter output showing excellent balancing in the split power.

devices. To increase the contrast a completely different set of irradiation parameters have been used. In particular, it has been found that waveguide writing with a higher repetition rate ($\sim$ 1MHz) and without any beam shaping optics can provide a significant increase in the refractive index change. The writing laser is a mode-locked cavity-dumped Yb:KYW laser producing 350-fs pulses at 1030 nm, with energy up to 1 µJ and 1 MHz repetition rate [65]. The writing beam is the second harmonic of such laser and is focused into the sample by a 50× objective with 0.6 NA, using an average power of 90 mW. The sample is moved at a speed of 100 µm/s by a three-axis air-bearing stage. The use of the second harmonic improves the waveguide homogeneity (thus reducing the propagation losses) due to the increased photon energy that reduces the nonlinearity in the absorption mechanism; in fact, given the large bandgap of fused silica the absorption of photons at the fundamental wavelength is highly nonlinear and therefore even small fluctuations in the irradiation power can cause relevant variations in the waveguide formation mechanism. The obtained waveguides display a refractive index contrast $\Delta n \sim 6 \times 10^{-3}$. It should be pointed out that the increased refractive index contrast is achieved at the expenses of some damaging of the glass close to the waveguide. As shown in Fig. 4a, the waveguide cross-section displays a fairly elongated shape (as mentioned no beam shaping optics is used) where the upper half (pointed by a red arrow in the figure) is not transparent while the lower half (pointed by a green arrow) is the guiding portion. The dark side of the waveguide seems to be necessary to achieve high refractive index changes since, every time a processing window providing completely transparent waveguides was found, the refractive index change was invariably lower.

The waveguides obtained in this irradiation regime work particularly well in the near-infrared with a single guided mode at 1.5 µm wavelength with 11-µm diameter (Fig. 4b) and 0.8 dB/cm propagation losses. The increased refractive index change keeps the bending losses to a reasonably low value for curvature radii as small as 20 mm (Fig. 4c). This opens the way to the fabrication of curved waveguides and of more complex devices in a small footprint. As a first example a Y-junction splitter has been fabricated with a curvature radius of 30 mm (Fig. 4d). The device is 2.4 mm long and achieves a waveguide separation at the output of 100 µm. The input light at 1.55 µm wavelength is equally split in the two output waveguides as shown in Fig. 4e.

3. Femtosecond laser microfluidic channel fabrication

3.1. Fundamental physical mechanisms

Only two materials have been used, up to now, for microchannel fabrication by the FLICE technique: fused silica and Foturan (Schott). The work on Foturan has been reviewed elsewhere [66], therefore we will concentrate in the following on the results obtained in fused silica. The increased HF etching rate of fused silica following femtosecond laser irradiation is due to the combination of two mechanisms. A first one is related to the decrease of the Si-O-Si bond angle induced by the hydrostatic pressure or compressive stress created in the irradiated region [67]. This explanation is particularly suited for the low intensity

regime, corresponding to the formation of optical waveguides; in fact, under these conditions, the etching rate has been shown to be proportional to the increase of the refractive index [68]. However, in this regime only a very modest increase in the etching rate is obtained after irradiation. A second mechanism, active for high intensity irradiation and giving a much higher etching selectivity, is the formation of self-ordered nanocracks, perpendicular to the laser polarisation direction [37]. The physical processes underlying the formation of nanocracks have been studied in detail in [69, 70] and involve the following transient nanoplasmonic model:

i) in the focal volume, hot spots for multiphoton ionization occur due to the presence of defects or color centers;
ii) such hot spots evolve into spherically shaped nanoplasmas over successive laser pulses due to a memory effect [71], equivalent to a reduction of the effective bandgap in the previously ionized region;
iii) field enhancement at the boundaries of the nanoplasma droplets results in asymmetric growth of the initially spherical droplets, in a direction perpendicular to the laser polarization, leading to the formation of nanoellipsoids, which eventually grow into nanoplanes;
iv) the nanoplanes are initially randomly spaced; when the electron plasma density inside them exceeds the critical density, they become metallic and start influencing light propagation in such a way that they assemble in parallel nanoplanes spaced by λ/n, where λ is the wavelength of the femtosecond writing laser and n the refractive index of the medium.

One particular feature of this process, which is very important for applications, is that nanoplanes formed in adjacent focal volumes displaying a lateral offset tend to be coherently linked, resulting in a self-alignment of the planes (that become aligned nanocracks if a suitable fluence is used in the irradiation process). This simple model highlights some peculiar features of the FLICE process:

i) it is not a single-pulse effect, but it relies on the cumulative action of multiple femtosecond laser pulses impinging on the same spot; it is therefore important to select the right combination of intensity and translation speed during the writing process;
ii) the process critically depends on the alignment of the writing laser polarization with respect to the translation direction [72]; when the polarization is aligned perpendicularly to the translation direction, then the nanocracks (which are perpendicular to the polarization) are directed along the channel axis, favouring the diffusion of the etchant; if on the other hand the polarization is parallel to the translation direction, then the nanocracks are perpendicular to the channel axis and etchant diffusion is blocked.

Based on this model, we can now understand the FLICE process as follows: during the etching process the nanocracks act as channels for the diffusion of the acid deeper into the fused silica, starting from the end face of the sample. Hence the etching process is a combination of two simultaneous phenomena: the diffusion of the acid along the irradiated region and the etching of the fused silica that gets in contact with such acid. Therefore, the etching process should not be thought as the acid carving its way by progressively removing the irradiated material but as a fast diffusion of acid in the irradiated region that causes an etching of material along the diffusion path. This also explains why the etching process is self terminating, due to the exhaustion of the HF acid in the depth of the etched microchannel and to the difficulty in refreshing it.

3.2. Microchannel properties

As in waveguide writing, also in the FLICE technique the microfluidic channels are defined inside the glass substrate by translating it along (longitudinal geometry) or perpendicularly (transversal geometry) to the laser beam propagation direction. Also for the microchannels, the transverse geometry has superior flexibility and allows defining structures of arbitrary length and shape, but has the disadvantage of generating channels with highly asymmetric cross section (see Sect. 2.2), which is undesirable for microfluidic applications. Several solutions to this problem have been proposed and implemented in the context of microfluidic channel fabrication. A first approach consists in stacking side by side different laser affected zones, created by subsequent scans of the substrate, to obtain a nearly symmetric cross section of the modified volume [67]. This solution uses efficiently the laser power but needs multiple scans and longer processing time; in addition, it gives rise to channels with irregular rims, which follow the periodicity of the scans. An alternative approach involves shaping the focal volume by using either a slit [73] or a cylindrical telescope [74], as previously described for optical waveguides (see Sect. 2.2). More recently, a spatio-temporal focusing technique has been proposed [75], which is based on the spatial dispersion of the spectrum of the writing beam; in this way the pulse has the minimum duration only in the focus of the objective and this reduces the confocal parameter of the beam, producing spherical voxels.

Here we describe microchannels fabricated by astigmatic beam shaping [74]. Pulses from a regeneratively amplified Ti:sapphire laser (800 nm, 150 fs, 1 kHz) with 3-μJ energy are shaped by a cylindrical telescope and focused below the surface of the fused silica sample by a 50× microscope objective ($NA = 0.6$, focal length $f = 4$ mm). The laser beam is polarized orthogonally to the translation direction and the sample is moved at a 20 μm/s speed. Following the irradiation, the sample is etched for 3.5 h in a solution of 15% HF in water, immersed in an ultrasonic bath. Figure 5 shows examples of cross sections of the resulting channels at different depths with respect to the sample surface, highlighting the reproducibility of the process and its 3D capabilities. The combination of astigmatic beam shaping and isotropy of the etching process results in nearly perfect circularity of the channel cross section, which is not easy to achieve by other microfabrication techniques. For a channel diameter of 80 μm, the estimated average roughness is of the order of 200 nm.

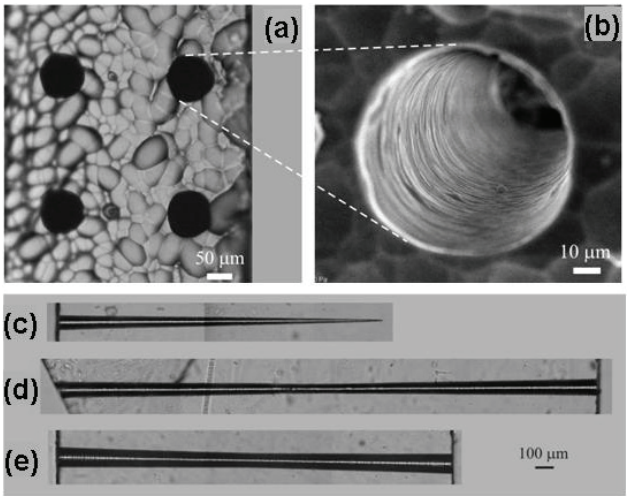

Figure 5 (a) End-face microscope image of a 2 × 2 matrix of microchannels; (b) SEM image of one channel; (c) top view of a dead-end microchannel; (d,e) top views of two-sided etched microchannels with different degrees of overlap.

The FLICE technique lends itself to the fabrication of both surface channels [67] and directly buried channels. In the first case, no practical limitations exist on the channel length and shape, as well as on the microfluidic circuit layout. The second case is however more appealing, since it avoids the chip sealing step and exploits the 3D capabilities of the FLICE technique. With directly buried channels, however, one is faced with limitations in channel length, shape and aspect ratio. In fact, etching of fused silica occurs through the reaction: $SiO_2 + 4\ HF \rightarrow SiF_4 + 2\ H_2O$. As the channel is progressively produced starting from the end face, it is necessary to remove the reaction products and provide fresh acid, which has to diffuse along the channel. With increasing channel length, the amount of fresh acid able to reach its end reduces and the etch rate gradually decreases [76, 77]. This limits the maximum achievable channel length and also results in microchannels with conical shapes, with larger radius at the channel entrance as compared to the buried end (see Fig. 5c). The cone apex angle α depends on the ratio between the etching rate of non-irradiated fused silica and the diffusion rate of the acid in the irradiated channel. There is usually a trade-off between microchannel aspect ratio and length. Indeed, a low HF concentration [67, 76] decreases the etch rate and results in higher aspect ratio but shorter channel length; on the other hand, high HF concentration [74] results in a lower aspect ratio, due to a faster lateral etching, but delays the self termination of the etching process and increases the channel length.

Currently, the longest dead-end channels fabricated by FLICE are ≈ 1.8 mm-long, and have an aspect ratio (length to diameter ratio) of ≈ 20. It is possible to obtain longer channels by etching from two sides. According to the degree of overlap, different channel shapes can be obtained, such as a longer one with a narrow passage in the middle (Fig. 5d) or a shorter one with an almost uniform cross section (Fig. 5e) [64]. The former has a 3 mm length with an entrance diameter of 90 µm and a waist diameter of 50 µm, while the latter has a 2.2 mm length with 110 µm diameter at the ends and 90 µm at the waist. The capability of creating tapered channels is a unique feature of FLICE and can be of use for some applications (see Sect. 4.5).

A method to compensate for the conical shape in a single-side etching process consists in irradiating a reverse cone with respect to the one normally obtained after etching [78]. The concept behind this fabrication approach is shown in Fig. 6 and consists in irradiating a conical spiral, as that represented in Fig. 6a, forming a laser-modified conical surface, which is complementary to the cone that is created when etching a straight line. The laser polarization is always orthogonal to the cone axis. The expected result is shown in Fig. 6b, where the blue cone is that of typical channel etched starting from a straight line, while the red line represents the conical irradiation, which would compensate for this effect, and the dotted line shows the expected cylindrical microchannel. The spiral periodicity Λ is chosen such that there is sufficient overlap between two subsequent laser irradiated arcs. It is worth noting that, as mentioned in Sect. 3.1, the nanocracks, that are formed in the irradiation of successive overlapping arcs, are naturally self-aligned, thus providing effective nanopaths for the acid diffusion in the irradiated region. Given the much longer time that it takes to irradiate the spiral structure, microfabrication is

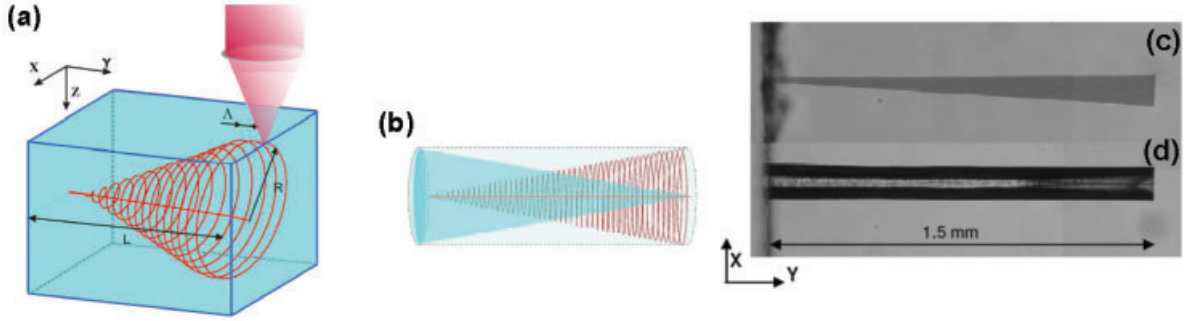

Figure 6 (online color at: www.lpr-journal.org) (a) Schematic diagram of a conical spiral inscribed into the substrate; (b) representation of a conical microchannel (blue), of the compensating conical spiral (red) and of the final cylindrical microchannel (grey). (c) Microscope image of the conically irradiated region and (d) final microchannel after the etching process.

performed by a high-repetition rate laser. We use the second harmonic (515 nm) of a cavity-dumped Yb:KYW oscillator providing 350-fs laser pulses at repetition rates up to 1 MHz [65]. With 150 nJ pulse energy, 600 kHz repetition rate and focusing with a 0.6 NA objective, it is possible to create straight microchannels with irradiation speeds up to 1 cm/s, i. e. nearly three orders of magnitude higher than with the 1 kHz laser. This allows to irradiate a spiral in approximately the same time that it takes to irradiate a straight line with the 1 kHz laser. By irradiating in the glass a conical spiral (Fig. 6c) with suitable angle, it is possible to obtain a dead-end etched channel with nearly uniform cross section (Fig. 6d) and to fabricate uniform microchannels with 4-mm length and constant 90-µm cross section by double side etching. In addition, with its unique control over the channel cross section, this approach allows also the fabrication of more complex structures, such as microchannels with access holes, interconnecting channels, microchannel adapters, and O-grooves [78].

Recently KOH was proposed as an alternative to HF for highly selective etching of femtosecond laser irradiated microchannels [79]. Experiments were performed using an highly concentrated aqueous KOH solution (10 M, corresponding to 35.8%) at 80 °C. The length saturation behaviour typical of fused silica etching in HF was not observed and the etching selectivity remained almost constant regardless of the etching time. It was therefore possible, using prolonged etching (60 h) in KOH, to fabricate microchannels as long as 1 cm with less than 60 µm diameter, corresponding to an aspect ratio of almost 200. The reason for this enhanced selectivity in KOH is not yet fully understood, but it is attributed to the structural changes induced in SiO_2 by the femtosecond laser irradiation when the high pressures and temperatures produce silicon-rich structures, i. e. an excess of Si-Si bonds [80]. Since KOH is a common etching agent for silicon but minimally attacks silica, one can expect highly selective etching of the laser irradiated volume. Despite the rather long etching times, thus, KOH overcomes some of the problems of HF and may, with further optimization, significantly boost the performance of the FLICE technique.

Femtosecond laser technology provides the exciting opportunity of using the same system for the fabrication of both microchannels and optical waveguides, and has the capability of easily integrating both structures in the same substrate, exploiting 3D geometries. One of the first examples of such integration is shown in Fig. 7 [64]. A 2.2-mm long microchannel is fabricated in a fused silica substrate by the FLICE technique using the 1 kHz Ti:sapphire laser with astigmatic beam shaping, as described above. The same laser is also used to inscribe three optical waveguides, spaced by 200 µm, perpendicular to the channel in its middle.

This represents an example of a basic optofluidic device completely fabricated by femtosecond laser technology. Its capability of selectively addressing the content of microchannels is demonstrated by filling them with a solution of Rhodamine 6G in ethylene glycol. When coupling 543 nm light in one waveguide by an optical fiber, yellow fluorescence is visible from the microfluidic channel (Fig. 7b).

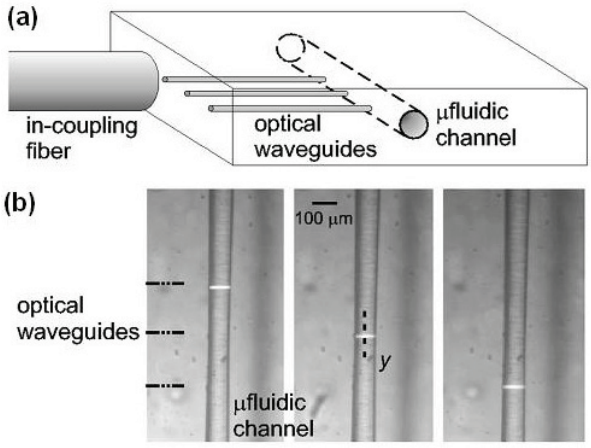

Figure 7 (a) Schematic of the waveguides crossing the microfluidic channel; (b) microscope image of the microfluidic channel with the fluorescence excited by the optical waveguides, which are not visible due to the low refractive index change and scattering losses.

No stray light coming from waveguide scattering reaches the microfluidic channel, demonstrating the high spatial selectivity of the excitation. Coupling each of the three waveguides provides a fluorescent signal at three different points of the microfluidic channel (see the three panels in Fig. 7b). This demonstrates the possibility of parallel multiple sensing at different positions in the microchannel. In the next section we will give an example of application exploiting this multipoint excitation capability.

4. Applications of femtosecond laser microfabrication to optofluidic devices

Having introduced the "tools of the trade" of femtosecond microstructuring, namely waveguide writing and microchannel fabrication, in this section we present examples of their application to optofluidics, for the sensing and manipulation of biomolecules and cells confined in microchannels. In some of the cases that will be presented, femtosecond laser waveguide writing is used for the integration of optical waveguides (Sect. 4.1) and more complex photonic devices (Sect. 4.2 and Sect. 4.4) on LOCs fabricated by conventional techniques. Here the laser is employed as a post-processing tool, to add the optical sensing capability to a device that has already been optimized for microfluidic functionality. In other examples (Sects. 4.3, 4.5, and 4.6) femtosecond laser microstructuring is used for the fabrication of the complete optofluidic device, including both optical waveguides and microchannels, integrated in a 3D arrangement.

4.1. DNA fragments separation by microchip capillary electrophoresis

One of the most powerful methods for the analysis of biomolecules is capillary electrophoresis (CE) [81], in

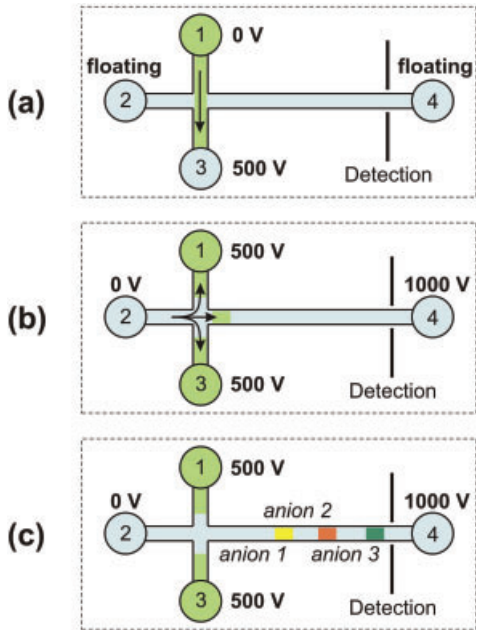

Figure 8 (online color at: www.lpr-journal.org) Scheme of a microfluidic channel network suitable for MCE, and different steps of the process: (a) filling of injection channel; (b) microfluidic plug injection; (c) plug separation.

which the molecules are separated in a thin channel as a result of their different mobility under an applied electric field. This technique is normally performed in a glass capillary filled with a buffer (sieving matrix), resulting in very high sensitivity and sorting accuracy, but at the expense of a bulky equipment and rather long separation times. CE is particularly suited for on-chip integration [2, 13], since electrokinetic flow can be used to move and mix liquids, thus avoiding the need to integrate pumps and valves. Microchip CE (MCE) is very promising for clinical applications, since it allows one to perform genetic tests to diagnose a variety of diseases, both exogenous (such as bacterial or viral infections) and endogenous (detection of mutated DNA sequences related to cancer or genetically inherited diseases) [82].

The schematic structure of a MCE chip is shown in Fig. 8. It consists of two channels crossing at 90°, the injection channel and the separation channel. Each channel is equipped with access holes at its end, where suitable electrodes allow applying voltage differences to the channels content. Separation of a mixture of different biomolecules occurs according to the following steps:

i) first the injection channel is filled, using electrokinetic flow, with the analyte molecules (Fig. 8a);
ii) then by a rapid switching of the voltages, a microfluidic "plug", corresponding to the intersection volume between the channels, is injected in the separation channel (Fig. 8b);
iii) the analyte species contained in the plug move at different speeds v, according to the expression $v = \mu\mathscr{E}$, where $\mathscr{E}$ is the electric field inside the channel and μ the so-called electrophoretic mobility, depending on size and charge of the molecules. The separated species are finally identified on the basis of their relative arrival times at the detection point (Fig. 8c).

To achieve high resolution MCE, it is necessary to suppress the electro-osmotic flow (EOF) and to fill the channel with a suitable sieving matrix. EOF is typical of glass substrates and occurs due to the formation of a double layer of electrical charges at the microchannel walls [83]. Such layer moves under an applied electric field and contributes to the electro-kinetic mobility. However, the EOF depends strongly on the quality of the microchannel walls, so that small defects in their surface will create "turbulences" in the EOF that will affect the MCE experiment by broadening the injected plugs. High quality MCE thus requires that EOF is suppressed by coating the channel with a suitable polymer that shields the surface charges. In addition, the channel must be filled with a sieving medium which is able to induce a size-dependent separation of molecules which would otherwise have very similar mobility.

Different detection schemes are possible in MCE, but among them the most popular is LIF which, being a background-free technique, allows the measurement of very low analyte concentrations. To perform this measurement the analytes are first labeled with a fluorescent molecule, then the CE separation is performed and finally fluorescence is excited and collected at the detection point. Femtosecond laser waveguide writing can be used as a post-processing tool to integrate inside MCE chips optical waveguides intersecting the microfluidic channels at various locations, in order to excite their content with high spatial selectivity [84–87].

Figure 9 shows a scheme of an MCE chip with integrated optical waveguides. It is based on a commercial fused silica LOC (LioniX BV) manufactured by photolithography followed by wet etching and then sealed by a cover glass slab. The actual microfluidic circuit (Fig. 9b) has the classical cross design shown in Fig. 8; however, the channels are folded in order to reduce the chip footprint. The microchannels are located 500 µm below the chip surface and have a rounded rectangular cross section with 100 µm width and 50 µm height. The MCE chip is inserted in a commercial cartridge providing reservoir connections and electrical contacts. The entire on-chip flow is computer-controlled by switching the voltages applied to the reservoirs. Optical waveguides were inscribed towards the end of the separation channel (approximately 3 cm from the injection cross) using a 1-kHz amplified Ti:sapphire laser [84]. Employing astigmatic beam shaping, an elliptical cross section of the written waveguide was obtained, with a major diameter of ~ 50 µm in the vertical direction, in order to excite the maximum possible volume of the channel, while the minor diameter in the horizontal direction is ~ 12 µm in order to retain a high spatial resolution along the flow direction. As described in Sect. 2.3, the waveguides display propagation losses of the order of 0.5–0.9 dB/cm throughout the visible range, which are fully acceptable for sensing applications. Alignment of the waveguides with respect to the microchannels is achieved with a positioning accuracy better than 2 µm in the depth direction. To demonstrate the high spatial selec-

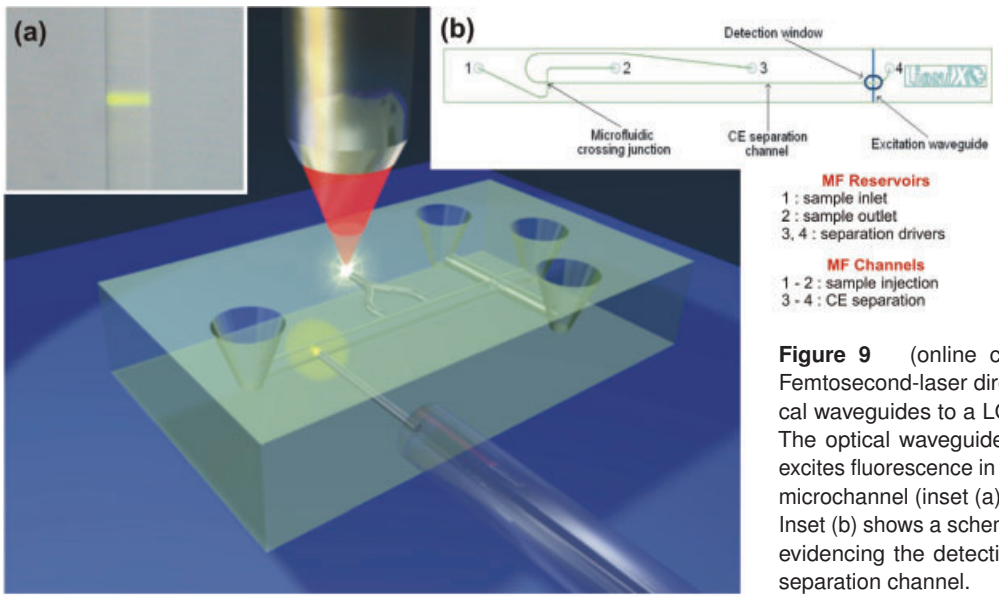

Figure 9 (online color at: www.lpr-journal.org) Femtosecond-laser direct writing is used to add optical waveguides to a LOC device designed for MCE. The optical waveguide, coupled to an optical fiber, excites fluorescence in a highly localized region in the microchannel (inset (a)), resulting in on-chip sensing. Inset (b) shows a schematic of the actual MCE device evidencing the detection window at the end of the separation channel.

tivity of excitation through the femtosecond laser written waveguides, the channel was first filled with a solution of a fluorescent dye (Rhodamine 6G). Figure 9a shows that the excited fluorescence is highly localized, confirming the very low leakage out of the waveguide, and extends across the whole channel width, due to the relatively low divergence of the waveguide mode. Femtosecond laser writing thus enables the integration of a "photofinish" at arbitrary positions in the separation channel. To achieve even higher integration, the fluorescence can be collected by a high numerical aperture (NA $= 0.5$) optical fiber, at 90° with respect to the excitation waveguide, resulting in a compact and portable setup [84, 86].

This optofluidic chip was used for MCE separation and detection of a commercial DNA ladder consisting of 17 double-stranded fragments with sizes in the range of 50–3000 base-pairs (bp) [87]. Prior to this experiment, the inner walls of the microchannel network were coated with a polymer [88] in order to suppress the EOF and to minimize adsorption of DNA molecules on the channel wall. Subsequently, the channels were filled with a sieving gel matrix [89] in order to maximize the resolution of MCE separation. The intercalating dye SYBR Green I was added for fluorescent labelling. Excitation through the optical waveguide was provided by the 488-nm line from a continuous-wave Ar-ion laser and the LIF was detected by a cooled photon-counting photomultiplier tube (PMT), after spectral selection with band-pass filters. Recording the LIF measured by the PMT as a function of time during the MCE separation leads to the electropherogram shown in Fig. 10a.

Thanks to the highly spatially localized excitation through the integrated waveguide, background light was very low. As a result, a remarkably low limit of detection for DNA fragments analysis of ~ 2.1 pM was achieved [87], which surpasses previously reported values in setups using on-chip-integrated fluorescence monitoring [84, 90]. Optimization of the coating and sieving gel matrix led to excellent MCE separation of the DNA molecules under integrated

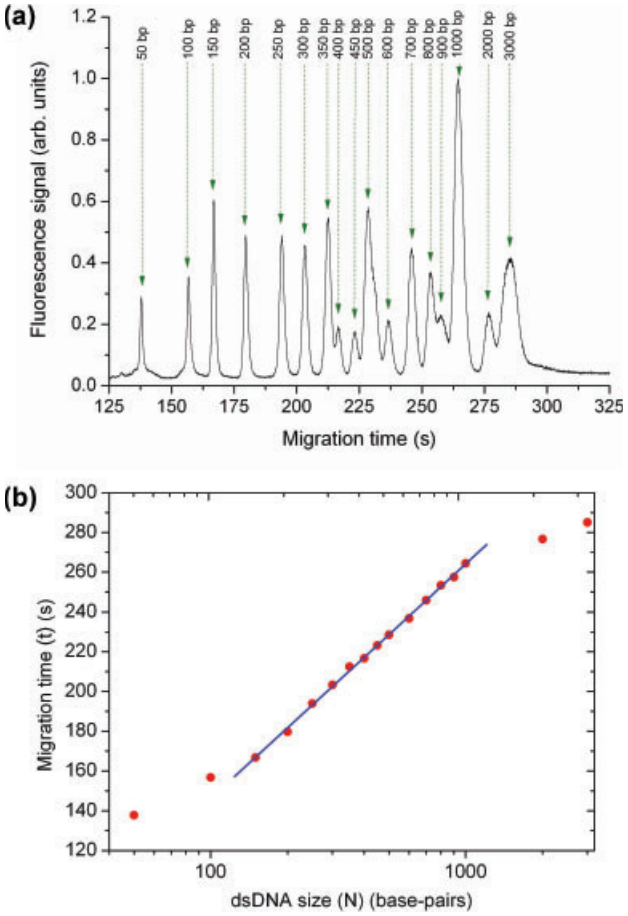

Figure 10 (online color at: www.lpr-journal.org) (a) Electropherogram depicting the fluorescence intensity under waveguide excitation as a function of time. The *a priori* known base-pair sizes of the 17 DNA-ladder molecules are indicated; (b) Migration time of the 17 CE-separated DNA molecules plotted against their *a priori* known base-pair sizes on a semi-logarithmic scale and a linear fit in the size range of 150–1000 bp [87].

waveguide excitation, see Fig. 10a. When plotting the temporal occurrence of the fluorescence peaks of the 17 molecules in Fig. 10a vs. their *a priori* known base-pair sizes, the two smallest (insufficient interaction with the sieving matrix) as well as the two largest DNA molecules (tendency to fold) exhibit clear deviations, while the peaks of all DNA molecules with sizes of 150–1000 bps, in the diagnostically relevant region, are resolved with a sizing accuracy higher than 99%, see Fig. 10b. This result is comparable to state-of-the-art performance in MCE-based DNA sequencing without integrated waveguides [82, 91].

Each measured fluorescence peak in the electropherogram is a convolution – along the flow axis – of the Gaussian-like waveguide mode-field, having a width Δx_{WG}, with the diffusion-induced physical width Δx_{MF} of the microfluidic plug. The resulting spatial plug widths Δx are related to the temporal electropherogram peak widths Δt as

$$\Delta x = \frac{L}{t}\Delta t = \sqrt{\Delta x_{WG}^2 + \Delta x_{MF}^2},$$

where $L = 3.6$ cm is the length of the separation channel and t (abscissa of Fig. 10a) is the migration time. In our experiment, the minimum electropherogram peak width was found to be $\Delta x = 248\,\mu$m (the very first peak in Fig. 10b). With $\Delta x_{WG} = 12\,\mu$m, we obtain $\Delta x_{MF} \gg \Delta x_{WG}$, i. e., the current spatial resolution is limited by the microfluidic plug width, while the obtained integrated-waveguide mode profile would allow for a 20-fold better resolution. Technological advances in the microfluidics, e. g. by improving the channel-wall coatings and sieving gel matrices, will eventually lead to smaller plug widths, thereby fully exploiting the monitoring resolution achieved with integrated optical waveguides.

These results demonstrate the capability of femtosecond laser writing to fabricate high quality optical waveguides in a fused silica MCE chip, which can excite with high spatial selectivity separated, fluorescently labelled molecules flowing in the microchannels. This approach is quite powerful because it allows the integration of photonic functionalities by simple post-processing of commercial LOCs, fabricated with standard techniques. This enables the development of highly integrated fluorescence excitation/detection schemes which could strongly increase the portability and compactness of the LOCs by overcoming the present limitation where microfluidic systems are coupled to macroscopic bulk optical detection systems. Having achieved this goal, we can now exploit the capability of femtosecond waveguide writing to inscribe multiple "photofinishes" along the separation channel, thus allowing parallel excitation at several positions along the channel. In several fundamentally important diagnostic applications two independent samples, each consisting of a number of differently sized DNA molecules, have to be monitored simultaneously, hence two excitation beams and detection of fluorescence signals at two wavelengths are required. These applications include, firstly, internal calibration of the set-up during a MCE experiment by adding to the sample under investigation a reference sample with several DNA molecules of known bp sizes, thereby making the experiment insensitive to environmental influences such as operating temperature, condition of the sieving gel matrix and inner wall coating of the microchannels, or changes of the applied electric field. Secondly, an unknown, potentially malign sample exhibiting single base-pair insertions or deletions can be separated together with its healthy counterpart, thereby providing unprecedented sizing accuracy to the experiment. Femtosecond waveguide writing, allowing the fabrication of several parallel waveguides which can interrogate the microchannel contents at multiple points, provides an effective solution to this problem. Here we propose a simple method for spatial and wavelength duplexing, which applies dual-point, dual-wavelength detection from a single detection window (DW) [92]. It does not require any external apparatus to separate the wavelengths, thereby allowing for fluorescence detection with a single, ultrasensitive PMT.

The layout of our optofluidic chip is presented in Fig. 11. A DW consists of a region in which two parallel femtosecond-laser-written waveguides carrying two different excitation wavelengths intersect the MCE separation channel in plane at two nearby locations with a mutual distance of 1 mm. The same experimental protocol and detection optics was implemented as described earlier.

When comparing an unknown sample, e. g. from a gene region under investigation for bp insertion/ deletion, with a reference sample, e. g. from the same gene region corresponding to a healthy person, the bp difference between the corresponding analyte DNA molecules would be small (1–2 bp), if any, thus challenging the resolution capabilities of standard MCE systems. Here we propose to determine these differences by exclusively labeling the two samples, flowing them against each other, and monitoring their separation with dual-point, dual-wavelength fluorescence excitation / detection through a single DW. If no insertion / deletion is present, the two species migrate with the same speed, but will nevertheless be optically separated due to the spatial separation between the two excitation waveguides in the DW.

For a proof of principle we used commercially produced single-stranded DNA primer molecules sized 19 and 20 nucleotides (nt), end-labeled with either Alexa Fluor 647 (AF647) or Cyanine 3 (Cy3). These two fluorophores can be selectively excited in the red (633 nm, coupled through WG1) and in the green (543 nm, coupled through WG2), respectively, without any sign of cross-excitation.

The two labeled DNA molecules were mixed and the resulting polychromatic mixture was resolved into the individual monochromatic DNA components by dual-point,

Figure 11 (online color at: www.lpr-journal.org) Layout of the optofluidic chip indicating the microfluidic reservoirs, channels, and the DW, comprising two waveguides crossing the MCE separation channel perpendicularly in plane [92].

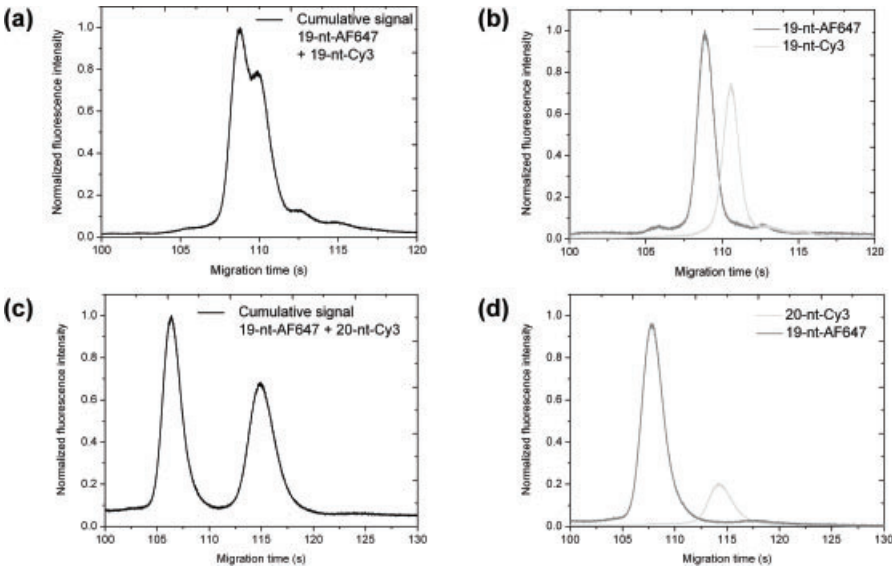

Figure 12 Electropherograms depicting the MCE separation of two fluorescently labeled DNA molecules: (a) cumulative signal during simultaneous dual-wavelength excitation of migrating 19-nt-AF647 and 19-nt-Cy3 molecules; (b) individual signals detected during single-wavelength excitation with only one of the two lasers switched on, temporally superimposed on each other; (c) and (d) the same for 19-nt-AF647 and 20-nt-Cy3 molecules [92].

dual-wavelength excitation in the MCE separation channel. Figure 12a depicts the corresponding electropherogram when separating a sample mixture of 19-nt-AF647 + 19-nt-Cy3. The two peaks separated by ~ 1.8 s correspond to the two species, each excited by the corresponding laser wavelength of 633 nm or 543 nm (provided by red and green He-Ne lasers, respectively) coupled into the adjacent waveguides. This is further confirmed by repeating the MCE separation twice, alternately turning off one of the lasers. The corresponding electropherograms displayed in Fig. 12b show a good match with the corresponding peak heights and positions in Fig. 12a. To visualize the case of single bp insertion / deletion, we repeat the experiment with a sample mixture of 19-nt-AF647 + 20-nt-Cy3. The corresponding electropherograms are shown in Fig. 12c, d, with an evidently larger peak separation of ~ 6.2 s.

A unique advantage of dual-point, dual-wavelength excitation is its capability of achieving MCE separation of equally sized, but differently labeled species, which naturally migrate at the same speed, by the inherent spatial separation of the two waveguides carrying the corresponding unique excitation wavelengths. The lack of perfect match in the peak positions and intensities between Fig. 12a, b and Fig. 12c, d is attributed to slight, unintentional differences in the experimental flow parameters. Nevertheless, using two femtosecond-laser-written waveguides, we demonstrate highly accurate detection of single-nucleotide insertion/deletion, as is relevant in genetic diagnostics – detection of anomalies in genetic samples obtained from a patient with respect to their healthy genetic counterparts.

4.2. Label-free sensing with Mach-Zehnder interferometers

Fluorescence detection, due to its background-free nature, provides the highest sensitivity, down to the single-molecule limit [93]. However, this approach suffers from laborious labelling processes that may interfere with the function of a biomolecule or living cell, or may prevent on-chip chemical reactions from taking place. On the other hand, the measurement of refractive index variations allows label-free sensing, detecting the analyte in its natural form without any alteration. This detection approach is particularly suited for monitoring the kinetics of transient processes without interfering with the reactions. Various monolithic optical devices for refractive index sensing have been proposed [94]; standard approaches, based on integrated optics, include Mach-Zehnder Interferometers (MZIs) [95], Young interferometers [96], and Bragg gratings [97]. These devices are fabricated by various techniques such as plasma vapour deposition, reactive ion etching, and also liquid-core waveguides [98]. Such methods are however only capable of producing 2D optical circuits. In addition, these devices typically exploit interaction between the evanescent field of the guided mode and the fluid in the microchannel, requiring long interaction lengths (millimeters to centimeters) for sensitive detection. On the other hand, several microfluidic applications call for spatially selective label-free detection, e. g. when molecules are separated in a microchannel by CE or when counting is required as in cell flow cytometry. In addition, spatially selective refractive index detection would enable multipoint sensing, e. g. for monitoring the reaction kinetics in chemical microreactors [99].

Here we employ femtosecond laser writing to fabricate a monolithic device capable of label-free and spatially-resolved optical sensing in a microfluidic chip. It consists of an MZI integrated with a microfluidic channel in a commercial LOC for MCE. The sensing arm of the MZI orthogonally crosses the channel, while the reference arm passes over it (see layout in Fig. 13) [100]. The device is capable of refractive index sensing with a spatial resolution of the order of the waveguide mode diameter (10–15 μm).

As a preliminary step to integration with the microfluidic channel, the MZIs were fabricated in a plain fused silica substrate, using the previously described high repetition rate Yb:KYW laser. This system provides waveguides with refractive index contrast $\Delta n \approx 5 \times 10^{-3}$, which is sufficient

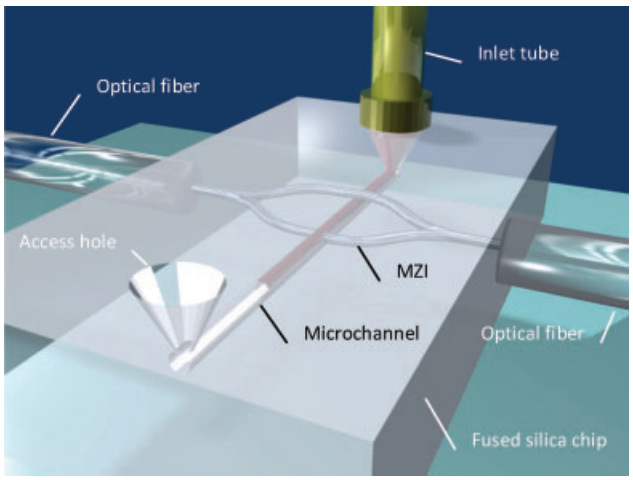

Figure 13 (online color at: www.lpr-journal.org) Schematic of the femtosecond-laser-fabricated microfluidic channel and integrated MZI. The sensing arm crosses orthogonally the channel, while the reference one passes over it [100].

for the fabrication of curved waveguides, splitters and MZIs. Unbalanced interferometers were designed, in order to detect fringes in the wavelength-dependent transmission when scanning a sufficiently broad spectral region with a tunable laser. The MZIs were integrated in a commercial LOC (LioniX BV) for MCE, similar to the one discussed in Sect. 4.1. The microchannels of this chip have a cross-section with 110 µm width and 50 µm depth and are buried at a depth of 500 µm from the surface. The MZIs are inscribed at the end of the separation channel, in the area evidenced by shading in Fig. 14a. The MZIs intersect the channel at a 90° angle in order to achieve spatially selective detection. The high spatial resolution comes at the expense of the sensing length, which is limited by the channel width. Therefore, to maximize the phase shift induced by the analyte, direct intersection of the sensing arm with the microchannel was chosen. In this way the sensing region is a cylinder with a height equal to the channel ($\sim 100\,\mu m$) and a base approximately equal to the waveguide mode size with a diameter of $\sim 15\,\mu m$. To enable only one arm intersecting the microchannel, the MZI was inscribed in a plane tilted by 7° with respect to the horizontal. The sensing arm of the MZI (which is chosen as the shorter one) orthogonally intersects the microchannel in its center (see Fig. 14, panel d), while the reference arm passes 20 µm above the microchannel (panel c). This tilted geometry of the MZI is necessary to achieve spatially selective sensing, since only one arm has to cross the channel. This is a clear example of an application where the 3D capabilities of femtosecond laser microfabrication are needed. In fact, it would have been very difficult to obtain this geometry with standard integrated optics technologies, which are intrinsically planar.

When one of the arms of the MZI crosses the microchannel, the transmission spectrum becomes

$$T = \frac{1}{2}\left[1 + \cos\left(\frac{2\pi}{\lambda}\left(n_0 \Delta s - (n_{\text{channel}} - n_0)\, L\right)\right)\right],$$

where Δs is the length difference between the two arms that can be tailored in order to obtain a fringe period smaller than the laser tunability range. Consequently, the transmission spectrum shows fringes with peaks positioned at

$$\lambda_m = \frac{n_0 \Delta s - (n_{\text{channel}} - n_0)\, L}{m}$$

where m is the fringe order.

The MZI will be affected by any change of the refractive index of the content of the microchannel (n_{channel}) with respect to the effective index of the guided mode (n_0) in the reference arm (the $(n_{\text{channel}} - n_0)/L$ term, where L is the microchannel width). If the content of the microchannel changes its refractive index by a quantity Δn, the transmission peaks will shift by

$$\Delta\lambda_m = -\frac{\Delta n \cdot L}{m}.$$

This shift can be accurately retrieved by a Fourier transform of the MZI transmission spectrum.

To characterize the sensitivity and the linearity of the interferometer response, the microchannel was filled with different concentrations of acqueous glucose-D solutions, and for each of them the spectral response of the optofluidic device was measured statically (see inset in Fig. 15). Figure 15 also shows the fringe shift of the transmission spectrum, calculated from the experimental data, as a function of glucose concentration (triangles). The scale on the right represents the corresponding refractive index variation of the solutions with respect to pure water, based on data reported in the literature. These measurements with glucose solutions allow a calibration of the device, correlating the fringe shift with the refractive index change in the microchannel, and give a device responsivity of 1500 nm/RIU.

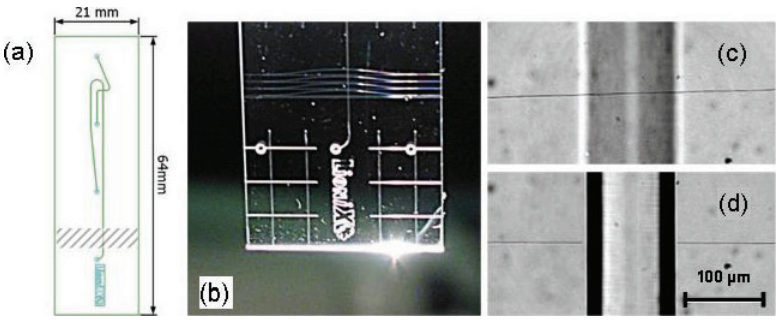

Figure 14 (online color at: www.lpr-journal.org) (a) Schematic of the commercial LOC for MCE (LioniX BV). MZIs are fabricated in a region at the end of the separation channel indicated by the shaded area. (b) Picture of the commercial LOC with 4 MZIs inscribed across a microchannel; the grid of microchannels at the bottom of the chip facilitates the sealing of the device and has no fluidic function. Microscope images of (c) the reference arm passing over the microchannel and (d) the sensing arm crossing it.

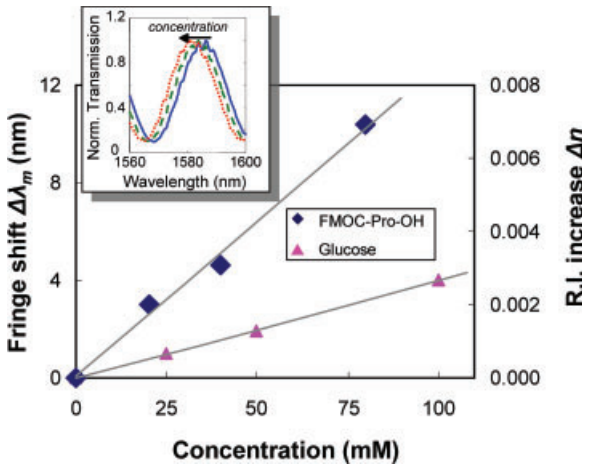

Figure 15 (online color at: www.lpr-journal.org) Measured fringe shift from spectral data for different concentrations of glucose-D in water (inset: 0 mM solid blue; 50 mM dashed green; 100 mM dotted red) and of the monopeptide FMOC-Pro-OH in ethanol; the correspondent refractive index increase is also shown in the right axis.

The standard deviation of the data taken from repeated measurements is $\sigma \approx 4.8 \times 10^{-5}$ RIU, therefore we can extrapolate a limit of detection of 1.5×10^{-4} RIU with a signal-to-noise ratio ≈ 3. Temperature fluctuations of the analyte (± 0.5 °C) are the limiting factor for device sensitivity, causing most of the noise in index measurements. In fact it can be estimated that an order of magnitude improvement in sensitivity could be achieved if the analyte were temperature stabilized.

Having assessed the performance of the device, it was used to detect biochemically relevant molecules such as peptides, used for drug synthesis in the pharmaceutical industry. Figure 15 shows the concentration dependent signal of the monopeptide FMOC-Pro-OH in ethanol (diamonds). The previous calibration, based on glucose solutions, quantitatively associates a refractive index increase to the measured fringe shift. Thus, the refractive index dependence on concentration for FMOC-Pro-OH can be determined, and is found to be linear with a slope of 8.2×10^{-5} RIU/mM.

These results demonstrate a compact and highly integrated interferometric device, directly fabricated on a LOC by post-processing, which allows refractive index sensing of the content of a microfluidic channel. The combination of label-free sensing and high spatial resolution is uniquely enabled by the femtosecond laser writing technique, which allows the fabrication of a 3D interferometer with only one arm crossing the microchannel.

4.3. Label-free sensing with Bragg gratings

As mentioned in the previous Section, label-free refractive index sensing of the content of a microfluidic channel is desirable for many applications. Maselli et al. have recently presented an example of an optofluidic device in fused silica, completely fabricated by femtosecond laser micromachining, which combines microfluidic channels and Bragg grating waveguides (BGWs) for refractive index sensing [101]. Writing the BGWs sufficiently close (less than 2 μm distance) to the very smooth microchannel walls enabled probing of the liquid-filled channel by the evanescent field of the waveguide mode and refractive index sensing through a shift of the narrow (~ 0.2 nm) BGW resonance.

The microfabrication was performed with the second harmonic (520 nm) [54] of an ultrafast Yb:fiber system, providing 300-fs pulses at 500 kHz repetition rate. The BGWs were fabricated by burst modulating the writing laser with an acousto-optic modulator [102], creating a continuous array of refractive index voxels that simultaneously provided low-loss waveguiding (~ 0.6 dB/cm), efficient mode coupling with standard optical fibers, and high-strength Bragg resonance (waveguide reflectance $R \approx 90\%$ and transmittance T ≈ -35 dB). The sample was translated in a direction parallel to the laser polarization to avoid waveguide birefringence and the Bragg wavelength was controlled by the sample translation speed. The microchannels were fabricated by the FLICE technique, using multiscan irradiation, thus leading to the formation of microchannels with rectangular 11-μm cross section and positioned 75 μm below the substrate surface. The fabrication parameters were optimized in order to minimize the microchannel roughness, and thus allow the smallest possible microchannel/BGW distance for maximum interaction of the evanescent wave with the fluid. Practically, the minimum achievable channel/BGW distance was 1.5 μm.

Different device geometries were investigated, according to the schemes reported in Fig. 16. The first topology (Fig. 16a) consists of a straight 25 mm long BGW parallel to a 10 mm long microchannel. The BGW consists of three serially cascaded segments, each one with a distinct Bragg wavelength. The central grating is positioned as close as possible to the channel, while the two side gratings, that have a slightly different Bragg wavelength, serve as references to compensate for temperature and strain variations. The second configuration (Fig. 16b) consists of a double S-bend waveguide positioned with the sensing BGW parallel to and slightly shorter than the adjacent microchannel. With this configuration, the sensor grating does not probe the starting and ending walls of the channel that induce back reflections

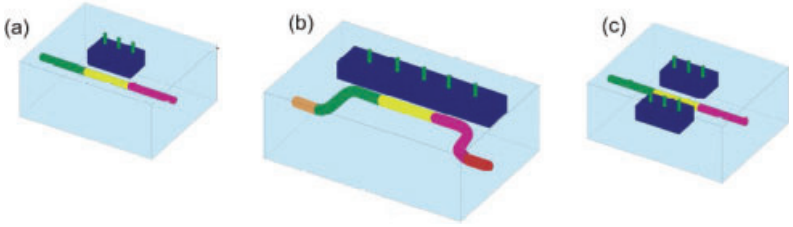

Figure 16 (online color at: www.lpr-journal.org) Schematics of microfluidic sensor geometries: straight BGW single channel (a), S-bend BGW single channel (b), and straight BGW double channel (c) [101].

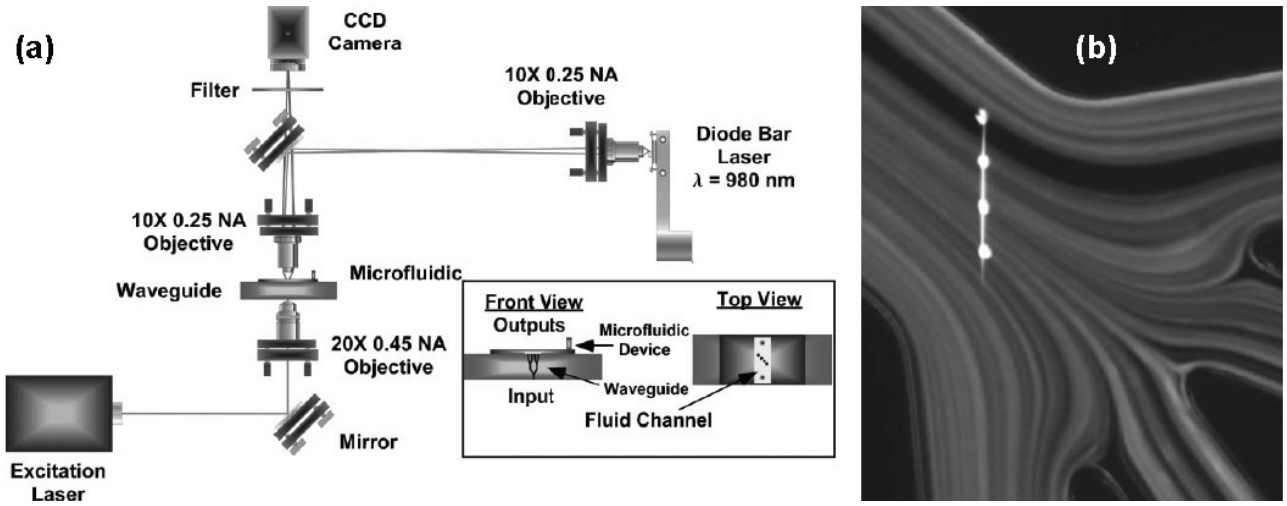

Figure 17 (a) Schematic of integrated FACS system based on optical waveguides combined with laser trapping. The trapping laser is aligned over the waveguide outputs. (b) Image of the junction in the microfluidic channel. The two outside channels are waste, while the central two channels are used for fluorescing and non-fluorescing sorted particles. The line focus of the laser diode bar and the four waveguide outputs are also shown [103].

and spectral distortions to the Bragg resonance. Finally the third design (Fig. 16c) is similar to the first, but with two microchannels placed parallel to and on opposite sides of the sensor BGW, with the objective of increasing the amount of evanescent field that penetrates into the microfluidic channels and thus improving the device sensitivity.

The three devices were tested by butt-coupling them to optical fibers: the input one is coupled to a broadband near-IR source (1530 to 1610 nm) while the output one is connected to an optical spectrum analyzer (OSA). Different analyte fluid filled the channels and induced shifts in the BGW resonance. The device sensitivity strongly depends on the refractive index of the sample to be measured and the highest value of 81 nm/RIU was obtained with the double-channel design and a sample refractive index approaching that of the fused silica substrate ($n = 1.458$). Given the present minimum λ shift of 0.01 nm resolvable by the OSA, the 81 nm/RIU response would offer a minimum resolvable refractive index variation $\Delta n_{\min}$ of $\sim 1.2 \times 10^{-4}$. Higher sensitivities can be achieved by: i) improvement of the channel wall roughness together with the extension of channels to wrap fully around the BGW; ii) narrowing the Bragg resonance linewidth; iii) engineering spectral defects with π-phase shifts.

4.4. Cell sorting

In this Section we present a fluorescence activated cell sorter (FACS) which allows to trap, detect and sort fluorescently labeled cells inside a microfluidic channel [103]. A first laser beam (the trapping beam) is used to trap cells inside the channel, while a second beam (the sensing beam) is used to excite their fluorescence and then to sort them into the desired channel by releasing, at a suitable time, the trapping beam.

The experimental setup of the FACS device is shown in Fig. 17a. The microfluidic network is fabricated in a polydimethylsiloxane (PDMS) substrate using soft lithography. The main channel is split into four channels (see Fig. 17b), two of which are used as waste and two for sorting purposes. A line focus, created inside the channel by relay imaging the 1×100 µm output of a diode laser bar (980 nm, 500 mW) is used to trap the particles in the channel. The PDMS chip lies on a fused silica substrate in which an optical waveguide network is fabricated by femtosecond laser writing. The network is a 1×4 splitter with 4 output beams of equal intensity, each with 6 µm diameter, spaced 30 µm apart. The waveguides are perpendicular to the channel and, when visible light is coupled into the splitter, 4 excitation points are available for cell fluorescence (see Fig. 17b). The four waveguide outputs are aligned with the line focus of the trapping beam.

Figure 18 shows an example of device operation, using 10 µm diameter Crimson Red labeled colloids. In this simple demonstration, shuttering the beam releases fluorescent colloids into outlet 1 while the non-fluorescent colloids are directed into channel 2. In Fig. 18 the first particle, which has been labeled, brightly fluoresces over a waveguide output. The emission radiation is detected using a photodiode and the trapping beam is subsequently blocked, causing this colloid to be sent into outlet 1. The second particle does not display fluorescence and thus is allowed to traverse the entirety of the trap, whereupon it is released into its respective streamline and exits into output 2. This enables sorting of particles that display distinct optical characteristics. This approach can be easily upscaled by exploiting the multipoint excitation capabilities of optical waveguides.

4.5. Flow cytometry

Detection, manipulation and sorting of single cells is required for several research and diagnostics applications in life sciences. Kim et al. [104, 105] have demonstrated an

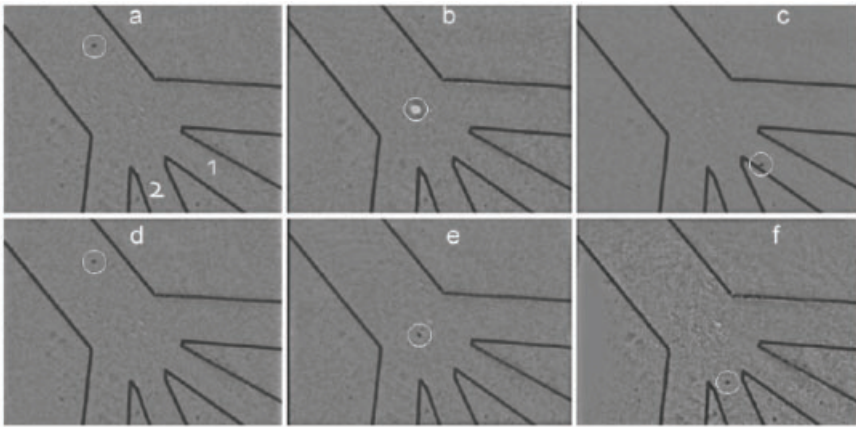

Figure 18 Images of a non-fluorescing colloid and a fluorescing colloid being sorted into different output streamlines, labelled 1 and 2 in frame a. Frames a-c show the path of the fluorescing colloid going into the outlet labelled 1. In frame b the colloid is fluorescing over the waveguide output aligned with outlet 1. Frames d–f show the non-fluorescing colloid path [103].

innovative approach to this problem by a glass based optofluidic device entirely fabricated by femtosecond laser microprocessing. The device consists of a three-dimensional flow-through microchannel fabricated inside bulk fused silica glass through the FLICE technique. The Venturi-type microchannel has circular cross section with diameter tapering from ≈ 100 µm at the entrance/exit ports to ≈ 10 µm at the flow neck, elegantly exploiting the intrinsic conical shape of the channels (see Sect. 3). The circular cross section of the flow channel neck is designed slightly smaller (≈ 1–2 µm) than the targeted cell diameter, in order to snugly fit individual cells. Thus, sample cells are self-aligned without resorting to additional flow focusing concepts, such as hydrodynamic [106] or elektrokinetic [107] focusing. Note that this device cleverly exploits the unique capability of femtosecond laser processing to fabricate channels with a tapering cross section (Fig. 19c). The microchannel is integrated with perpendicular optical waveguides written both parallel and normal to the top surface of the glass substrate. This approach enables effectively "confocal" cell detection and processing at the microchannel neck. Two different optical detection schemes were adopted: a passive setup measuring the transmitted light intensity of a He-Ne laser (Fig. 19a) and fluorescence emission using labelled cells and an Ar laser as excitation source (Fig. 19b).

In the first approach, the transmitted light intensity through the collecting waveguide exhibits distinct peaks due to the refractive index difference between cell and base solution. The second approach, due to its background-free nature, provides much higher contrast but requires cell pretreatment.

The performance of the device is verified by detecting red blood cells (RBCs) for volumetric flow rates up to 0.5 µl/min. The particle counting density (number of detected particles per second) in the microchannel is measured as a function of volumetric flow. The experimental counting density seems to follow the trend of the calculated counting density (estimated on the basis of the given particle con-

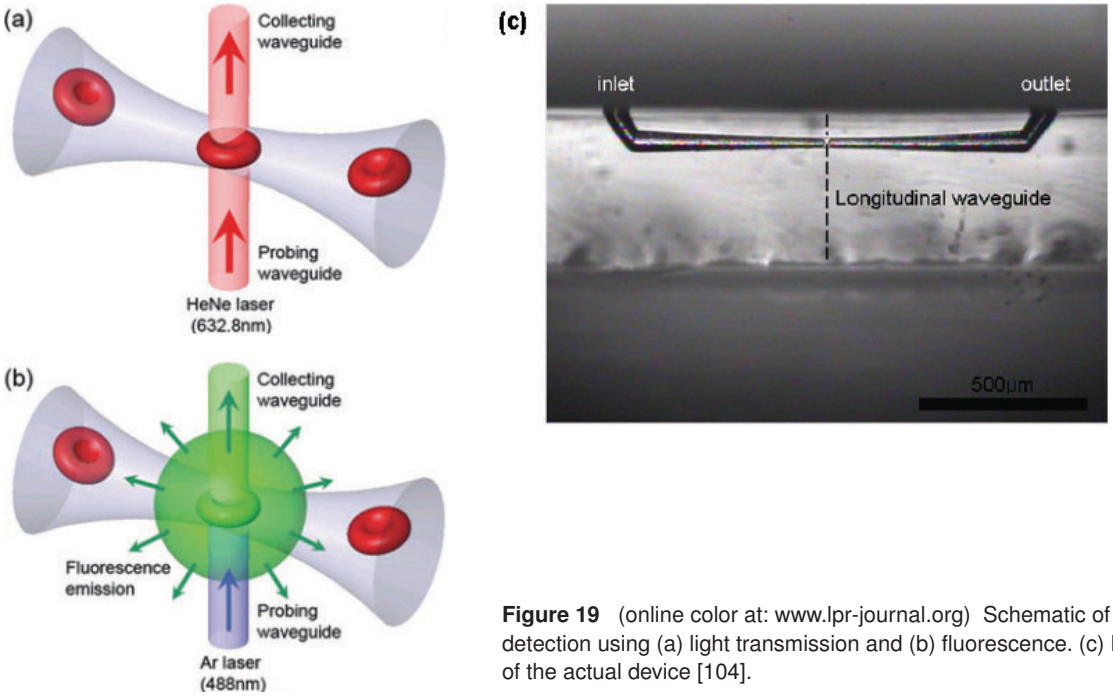

Figure 19 (online color at: www.lpr-journal.org) Schematic of the integrated cell detection using (a) light transmission and (b) fluorescence. (c) Microscope image of the actual device [104].

centration and volumetric flow rate), thus verifying that the proposed glass based optofluidic device can perfectly work as a cell/particle counter on a LOC.

Even though the operation range of this device as a cell/particle counter is somewhat lower than commercial cytometers (up to 1000 particles per second), it may be enough throughput for a cell/particle predetector of single cell manipulation processes on a chip, using the unique geometric and material advantages of the proposed device. The range can also be extended up to the order of cell counting efficiency of commercial cytometers using fine tuning of detection electric circuit and particle speed calibration.

4.6. Cell trapping and stretching

Here we report in detail on a monolithic optofluidic chip for cell trapping and stretching. Biophotonic devices based on optical forces are powerful tools for single cell study and manipulation without physical contact [108–110]. The exploitation of optical forces for analysis at single cell level provides significant information, opening new scenarios for the understanding of basic biological mechanisms and for the early detection of several diseases. In particular, the investigation of the viscoelastic properties of trapped cells and their response to the application of intense optical forces, able to cause a significant deformation of the cytoskeleton, is of great interest. It is widely recognized that alterations of the cytoskeleton deformability are present in many diseases and their measurement can be used as a reliable marker of the cell status [111].

Mechanical properties of single cells can be efficiently tested using a recently developed device based on optical fibers, named optical stretcher (OS) [112]. OS basic idea relies on a double beam laser trap [113] obtained with two counter-propagating beams [114, 115]. Increasing the laser power, the radiation pressure exerted by the two beams over the trapped cell surface leads to an elongation of the cell along the beam axis, providing useful information on the cell health. Although the effectiveness of the OS has been widely demonstrated, the typical set-ups, based on assembling optical fibers with glass capillaries or polymeric microchannels, present some criticalities mainly due to the fine and stable alignment required between discrete optical and microfluidic components [112, 114].

Differently from standard fabrication technologies, femtosecond laser micromachining is able to provide direct writing of both optical waveguides and microfluidic channels [64], ensuring extreme flexibility and accuracy, together with intrinsic 3D capabilities. It has thus been used to fabricate a monolithic optofluidic chip that allows performing mechanical analysis on single cells without physical contact and with high reproducibility (Fig. 20). The integrated chip is based on a fused silica glass substrate, thus providing high transparency for cell imaging, and represents a significant improvement in terms of stability, robustness and optical damage threshold over existing optical cell stretchers [116].

Both waveguides and microchannels are fabricated using a frequency-doubled, high repetition rate Yb:KYW laser.

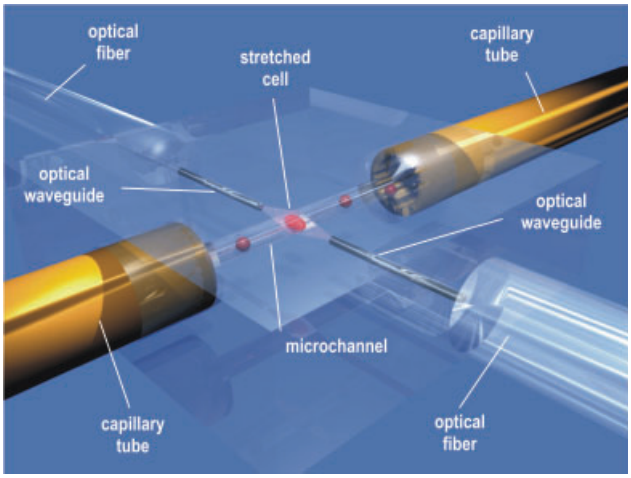

Figure 20 (online color at: www.lpr-journal.org) 3D rendering of the monolithic optical stretcher fabricated by femtosecond laser micromachining. The cells flowing in the microchannel are trapped and stretched in correspondence of the dual beam trap created by the optical waveguides. Connections to capillaries and optical fibers are also shown [116].

As discussed in Sect. 3.2, the FLICE approach provides an unprecedented freedom in designing 3D fluidic components by irradiating the substrate with beam trajectories more complex than just straight lines. Here we exploit this technique for two main purposes: i) fabrication of large access holes at the end of the microchannel, in order to enable a straightforward plugging of capillary tubes for connection with an external fluidic circuit; ii) shaping of the microchannel in the trapping region, in order to improve the imaging of the cell. Circular shape of the microchannel cross-section acts as a lens when imaging the trapped cells by a transmission microscope. This causes a deformation of the cell contour and complicates the determination of small elastic elongations during stretching. In order to avoid this problem we manufacture a square channel cross-section, by irradiating two coaxial helixes with rectangular cross-section one inside the other [117]. The microchannel is then terminated by two access holes that are obtained by irradiating coaxial helixes with circular cross-section, as shown in Fig. 21a. A 4.5 hours chemical etching in an ultrasonic bath with 20% of HF in water produces the microchannel as reported in Fig. 21b, which is 400-μm buried under the top surface, has a 2-mm length, a central rectangular cross-section of 85 μm × 75 μm, and two 800-μm-long access holes. While in the portions of the microchannel closer to the access holes the etching smooths out the corners of the rectangular cross-section, in the central portion the channel closely follows the irradiation path with a sharp rectangular shape as shown in Fig. 21c.

The same fabrication set-up used for pre-etching irradiation is employed, with lower fluence, to directly write optical waveguides into the fused silica substrate. The obtained waveguides have an intensity mode radius of 4.2 μm. Waveguide writing and pre-etching irradiation take place in the same fabrication step and so the accuracy in the alignment

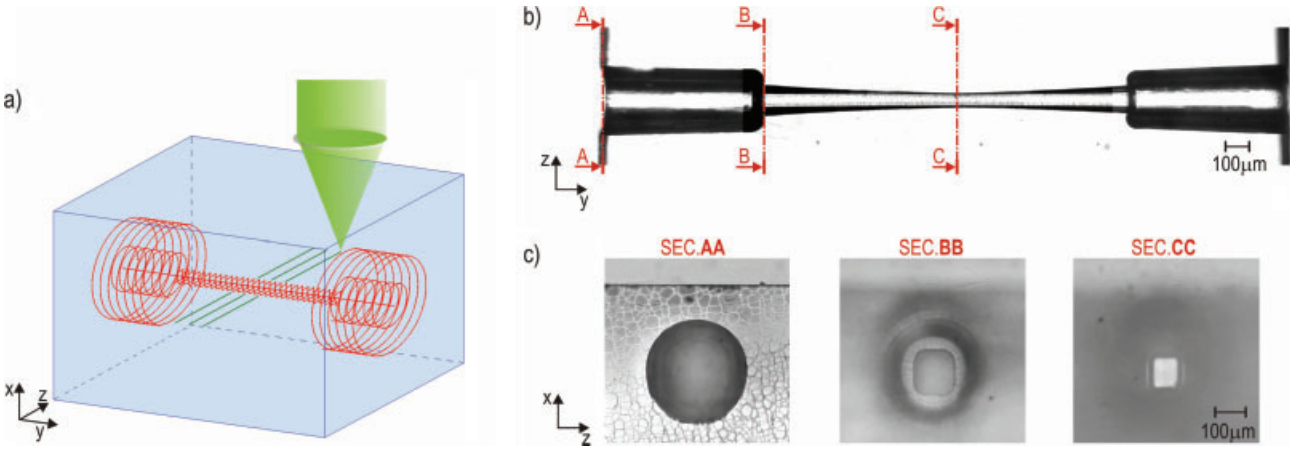

Figure 21 (online color at: www.lpr-journal.org) (a) Sketch of the pre-etching path for channel formation (red lines) together with the optical waveguides (green lines). (b) Picture of the fabricated microchannel after chemical etching. (c) Pictures of channel cross-section in different regions along the channel axis [117].

between the fluidic and the optical components corresponds to the accuracy of the translation stages, which is better than 100 nm. The optofluidic chip is connected to an external fluidic circuit through two capillary tubes glued into the access holes and it is coupled to the laser source by two bare-end optical fibers. The connected chip is then placed on a transmission microscope plate for imaging.

The integrated OS has been experimentally tested by trapping and stretching RBCs. Once the RBC suspension is flown into the microfluidic channel, optical trapping of single cells can be easily observed with an optical power in the trap of about 20 mW. In addition, by unbalancing the powers emitted by the two fibers, the trapped cell can be moved with good control along the beam axis. The square cross-section of the channel allows obtaining images of the trapped cells in which the contour is very well defined and can be automatically recovered. Figure 22a shows an image of the trapped cell where the recovered contour is indicated by a red line. By increasing the optical power in the trap up to 300 mW we observe a progressive stretching of the trapped cell as shown in Fig. 22b. Figure 22c reports a plot of the cell elongated dimension as a function of the optical power in the trap (P_C).

5. Outlook and conclusions

In this paper we have discussed the contribution of femtosecond laser micromachining to the field of lab-on-chips and optofluidics. We have shown that ultrashort laser pulses, besides their ability to inscribe waveguides and photonic devices (splitters, interferometers, gratings), can also be used, in combination with HF etching, to fabricate directly buried microfluidic channels. The main assets of femtosec-

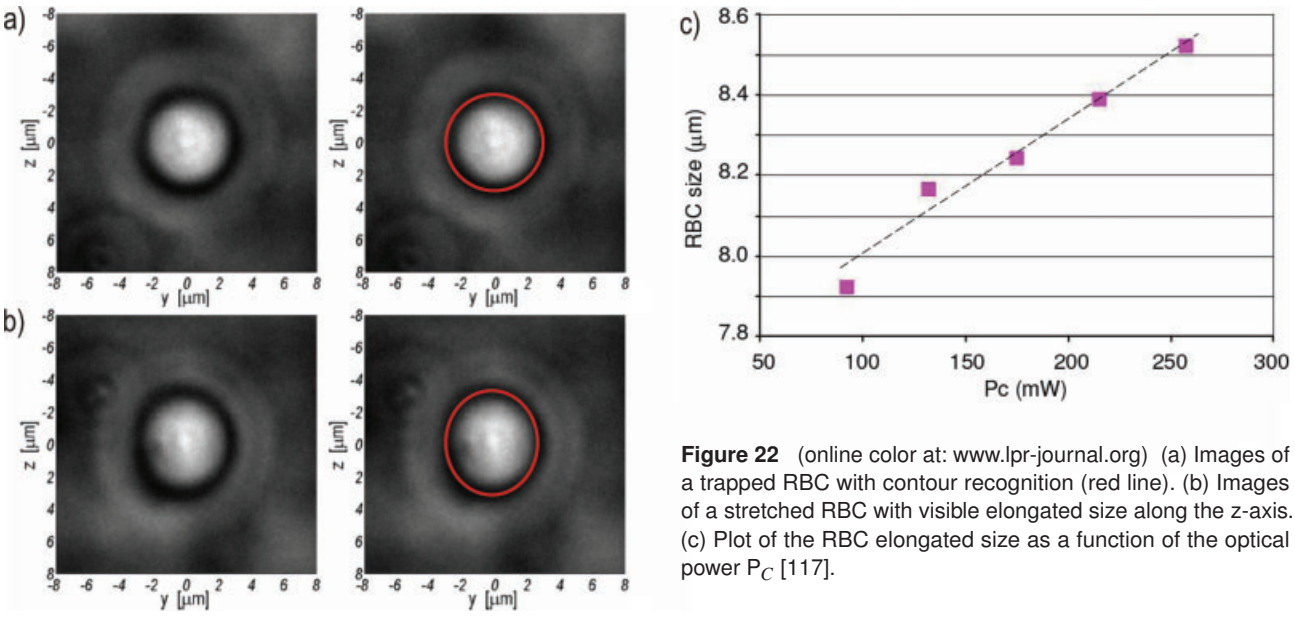

Figure 22 (online color at: www.lpr-journal.org) (a) Images of a trapped RBC with contour recognition (red line). (b) Images of a stretched RBC with visible elongated size along the z-axis. (c) Plot of the RBC elongated size as a function of the optical power P_C [117].

ond laser microfabrication are: i) being a direct-write technique, it can be used as a post-processing tool to add optical (and possibly fluidic) functionalities to a microfluidic device manufactured by conventional methods (see the MCE chips of Sect. 4.1); ii) its unique three-dimensional capabilities allows one to implement novel geometries, enabling the realization of devices with unprecedented features (see the 3D interferometer of Sect. 4.2); iii) the capability to produce both optical waveguides and microchannels allows one to design and fabricate a complete optofluidic device with extreme control on the components properties and device geometry (see the flow cytometer of Sect. 4.5 and the optical stretcher of Sect. 4.6). The field of femtosecond laser processing for optofluidics is still in its infancy and, in order to flourish, it will require a close synergy between microfabrication and biochemistry skills. However, femtosecond laser micromachining has already demonstrated to be an exciting playground to develop new optofluidic devices.

Acknowledgements. The authors would like to thank the many co-workers involved in the activities reported in the present paper; in particular we acknowledge relevant contributions by Rebeca Martinez Vazquez from IFN-CNR, Chaitanya Dongre from University of Twente, Nicola Bellini and Andrea Crespi from Politecnico di Milano, Krishna Vishnubhatla from Italian Institute of Technology, Hans van den Vlekkert and Rene Heideman from LioniX BV, Rob van Weeghel and Jasper van Weerd from Zebra Bioscience BV, Paul Watts from Hull University, and Ilaria Cristiani from University of Pavia. The authors would also like to acknowledge the financial support provided by the European Commission, through the FP6 project contract no. IST-2005-034562 [Hybrid Integrated Biophotonic Sensors Created by Ultrafast Laser Systems (HIBISCUS)], by the CARIPLO Foundation through the project "Materiali a memoria ottica passiva realizzati mediante cristalli liquidi in microstrutture tridimensionali", and by Regione Lombardia through the project MINILAB (ID MAN-18).

Received: 2 November 2010, **Revised:** 9 December 2010, **Accepted:** 16 December 2010

Published online: 8 February 2011

Key words: Optical waveguides, microfluidic channels, femtosecond lasers, microfabrication, waveguide writing, chemical etching, lab-on-a-chip, optofluidics, capillary electrophoresis, laser trapping.

Roberto Osellame received his M. Sc. degree in Electronic Engineering from the Politecnico di Milano (Italy) in 1996 and the Ph. D. degree in Physics from the Politecnico di Torino (Italy) in 2000. Since 2001 he is a Staff Researcher of the Institute of Photonics and Nanotechnology (IFN) of the Italian National Research Council (CNR) and a contract professor of the Politecnico di Milano. His research interests include integrated all-optical devices on nonlinear crystals and femtosecond laser micromachining of transparent material for the fabrication of photonic and optofluidic devices.

Hugo J. W. M. Hoekstra received the M. Sc. degree in Experimental Physics from the University of Amsterdam, in 1977. In 1984 he received his Ph. D. degree from the University of Groningen on a topic in the field of solid state physics. After two post-doc positions he joined the Integrated Optical Micro Systems group at the University of Twente, in 1988. He is specialized in optical sensors and theoretical aspects of optics.

Giulio Cerullo is Associate Professor of Physics with the Physics Department, Politecnico di Milano (Italy). His research activity has mainly focused on the physics and applications of ultrashort pulse lasers, covering a wide range of aspects. His current scientific interests concern generation of few-optical-cycle pulses, ultrafast spectroscopy with time resolution down to a few femtoseconds, nonlinear microscopy and optical waveguide writing by ultrashort pulses.

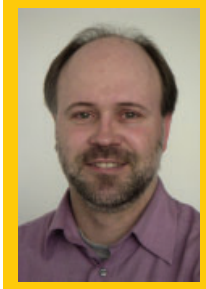

Markus Pollnau received his M. Sc. in Physics from the University of Hamburg, Germany and his Ph. D. in Physics from the University of Bern, Switzerland. In 2004, he was appointed a full Professor at the University of Twente, Enschede, The Netherlands. His scientific interests concern rare-earth-ion spectroscopy, solid-state, fiber, and waveguide lasers, and integrated optical devices. He has co-chaired the Conferences on Lasers and Electro-Optics in the United States (2006/2008) and Europe (2009/2011) and served as Topical Editor for the Journal of the Optical Society of America B.

References

[1] D. J. Harrison, K. Fluri, K. Seiler, Z. H. Fan, C. S. Effenhauser, and A. Manz, Science **261**, 895 (1993).
[2] A. T. Woolley and R. A. Mathies, Proc. Natl. Acad. Sci. USA **91**, 11348 (1994).
[3] S. C. Jacobson, R. Hergenroder, L. B. Koutny, and J. M. Ramsey, Anal. Chem. **66**, 1114 (1994).
[4] S. C. Jacobson and J. M. Ramsey, Anal. Chem. **68**, 720 (1996).
[5] A. J. de Mello, Nature **442**, 394 (2006).
[6] P. Yager, T. Edwards, E. Fu, K. Helton, K. Nelson, M. R. Tam, and B. H. Weigl, Nature **442**, 412 (2006).
[7] R. D. Reyes, D. Iossifidis, P. A. Auroux, and A. Manz, Anal. Chem. **74**, 2623 (2002).
[8] P. A. Auroux, D. R. Reyes, D. Iossifidis, and A. Manz, Anal. Chem. **74**, 2637 (2002).
[9] G. M. Whitesides, Nature **442**, 368 (2006).
[10] J. F. Dishinger and R. T. Kennedy, Anal. Chem **79**, 947 (2007).

[11] M. Madou, Fundamentals of Microfabrication: The Science of Miniaturization (Taylor and Francis Ltd, Boca Raton, 2002).
[12] E. Verpoorte, Lab Chip **3**, 42N (2003).
[13] A. H. J. Yang, S. D. Moore, B. S. Schmidt, M. Klug, M. Lipson, and D. Erickson, Nature **457**, 71 (2009).
[14] K. B. Mogensen, H. Klank, and J. P. Kutter, Electrophoresis **25**, 3498 (2004).
[15] H. C. Hunt and J. S. Wilkinson, Microfluid Nanofluid **4**, 53 (2008).
[16] K. B. Mogensen and J. P. Kutter, Electrophoresis **30,** S92 (2009).
[17] K. B. Mogensen, P. Friis, J. Hübner, N. J. Petersen, A. M. Jorgensen, P. Telleman, and J. P. Kutter, Opt Lett **26**, 716 (2001).
[18] R. Mazurczyk, J. Vieillard, A. Bouchard, B. Hannes, and S. Krawczyka, Sens. Act. B **118**, 11 (2006).
[19] J. Vieillard, R. Mazurczyk, C. Morin, B. Hannes, Y. Chevolot, P. L. Desbene, and S. Krawczyk, J. Chromatogr. B **845**, 218 (2007).
[20] B. Kuswandi, J. Nuriman, J. Huskens, and W. Verboom, Anal. Chim. Acta **601**, 141 (2007).
[21] K. B. Mogensen, J. El-Ali, A. Wolff, and J. P. Kutter, Appl. Opt. **42**, 4072 (2003).
[22] C. L. Bliss, J. N. McMullin, and C. J. Backhouse, Lab Chip **7**, 1280 (2007).
[23] C. L. Bliss, J. N. McMullin, and C. J. Backhouse, Lab Chip **8**, 143 (2008).
[24] D. Yin, D. W. Deamer, H. Schmidt, J. P. Barber, and A. R. Hawkins, Opt Lett **31**, 2136 (2006).
[25] D. Yin, E. J. Lunt, M. I. Rudenko, D. W. Deamer, A. R. Hawkins, and H. Schmidt, Lab Chip **7**, 1171 (2007).
[26] K. M. Davis, K. Miura, N. Sugimoto, and K. Hirao, Opt. Lett. **21**, 1729 (1996).
[27] S. Nolte, M. Will, J. Burghoff, and A. Tuennermann, Appl. Phys. A **77**, 109 (2003).
[28] A. Marcinkevicius, S. Juodkazis, M. Watanabe, M. Miwa, S. Matsuo, H. Misawa, and J. Nishii, Opt. Lett. **26**, 277 (2001).
[29] D. Psaltis, S. R. Quake, and C. Yang, Nature **442**, 381 (2006).
[30] C. Monat, P. Domachuk, and B. J. Eggleton, Nature Photon. **1**, 106 (2007).
[31] U. Levy, K. Campbell, A. Groisman, S. Mookherjea, and Y. Fainman, Appl. Phys. Lett. **88**, 111107 (2006).
[32] A. P. Joglekar, H. Liu, E. Meyhofer, and G. Mourou, A. J. Hunt, Proc. Natl. Acad. Sci. USA **101**, 5856 (2004).
[33] M. Ams, G. D. Marshall, P. Dekker, M. Dubov, V. K. Mezentsev, I. Bennion, and M. J. Withford, IEEE J. Sel. Top. Quantum Electron. **14**, 1370 (2008).
[34] D. Du, X. Liu, G. Korn, J. Squier, and G. Mourou, Appl. Phys. Lett. **64**, 3071 (1994).
[35] D. Rayner, A. Naumov, and P. Corkum, Opt. Express **13**, 3208 (2005).
[36] R. R. Gattass and E. Mazur, Nature Photon. **2**, 219 (2008).
[37] R. Taylor, C. Hnatovsky, and E. Simova, , Laser Photonics Rev. **2**, 26 (2008).
[38] K. Itoh, W. Watanabe, S. Nolte, and C. B. Schaffer, MRS Bull. **31**, 620 (2006).
[39] E. Glezer and E. Mazur, Appl. Phys. Lett. **71**, 882 (1997).
[40] S. Juodkazis, K. Nishimura, S. Tanaka, H. Misawa, E. G. Gamaly, B. Luther-Davies, L. Hallo, P. Nicolai, and V. T. Tikhonchuk, Phys. Rev. Lett. **96**, 166101 (2006).
[41] M. Streltsov and N. F. Borrelli, J. Opt. Soc. Am. B **19**, 2496 (2002).
[42] P. Dekker, M. Ams, G. D. Marshall, D. J. Little, and M. J. Withford, Opt. Express **18**, 3274 (2010).
[43] C. B. Schaffer, J. F. García, and E. Mazur, Appl. Phys. A **76**, 351 (2003).
[44] W. Chan, T. Huser, S. Risbud, and D. M. Krol, Opt. Lett. **26**, 1726 (2001).
[45] T. Gorelik, M. Will, S. Nolte, A. Tuennermann, and U. Glatzel, Appl. Phys. A **76**, 309 (2003).
[46] V. Apostolopoulos, L. Laversenne, T. Colomb, C. Depeursinge, R. P. Salath, M. Pollnau, R. Osellame, G. Cerullo, and P. Laporta, Appl. Phys. Lett. **85**, 1122 (2004).
[47] K. Miura, J. Qiu, H. Inouye, T. Mitsuyu, and K. Hirao, Appl. Phys. Lett. **71**, 3329 (1997).
[48] D. Homoelle, S. Wielandy, A. L. Gaeta, N. F. Borrelli, and C. Smith, Opt. Lett. **24**, 1311 (1999).
[49] C. B. Schaffer, A. Brodeur, and E. Mazur, Meas. Sci. Technol. **12**, 1784 (2001).
[50] C. B. Schaffer, A. Brodeur, J. F. Garcia, and E. Mazur, Opt. Lett. **26**, 93 (2001).
[51] K. Minoshima, A. Kowalevicz, I. Hartl, E. Ippen, and J. Fujimoto, Opt. Lett. **26**, 1516 (2001).
[52] R. Osellame, N. Chiodo, V. Maselli, A. Yin, M. Zavelani-Rossi, G. Cerullo, P. Laporta, L. Aiello, S. De Nicola, P. Ferraro, A. Finizio, and G. Pierattini, Opt. Express **13**, 612 (2005).
[53] R. Osellame, N. Chiodo, G. Della Valle, S. Taccheo, R. Ramponi, G. Cerullo, A. Killi, U. Morgner, M. Lederer, and D. Kopf, Opt. Lett. **29**, 1900 (2004).
[54] L. Shah, A. Arai, S. Eaton, and P. Herman, Opt. Express **13**, 1999 (2005).
[55] S. M. Eaton, H. Zhang, M. L. Ng, J. Li, W.-J. Chen, S. Ho, and P. R. Herman, Opt. Express **16**, 9443 (2008).
[56] R. Osellame, N. Chiodo, G. Della Valle, G. Cerullo, R. Ramponi, P. Laporta, A. Killi, U. Morgner, and O. Svelto, IEEE J. Sel. Top. Quantum Electron. **12**, 277 (2006).
[57] M. Will, S. Nolte, B. N. Chichkov, and A. Tünnermann, Appl. Opt. **41**, 4360 (2002).
[58] G. Cerullo, R. Osellame, S. Taccheo, M. Marangoni, R. Ramponi, P. Laporta, and S. De Silvestri, Opt. Lett. **27**, 1938 (2002).
[59] R. Osellame, S. Taccheo, M. Marangoni, R. Ramponi, P. Laporta, D. Polli, S. De Silvestri, and G. Cerullo, J. Opt. Soc. Am. B **20**, 1559 (2003).
[60] M. Ams, G. D. Marshall, D. J. Spence, and M. J. Withford, Opt. Express **13**, 5676 (2005).
[61] Y. Nasu, M. Kohtoku, and Y. Hibino, Opt. Lett. **30**, 723 (2005).
[62] R. R. Thomson, A. S. Bockelt, E. Ramsay, S. Beecher, A. H. Greenaway, A. K. Kar, and D. T. Reid, Opt. Express **16**, 12786 (2008).
[63] S. M. Eaton, H. Zhang, P. R. Herman, F. Yoshino, L. Shah, J. Bovatsek, and A. Y. Arai, Opt. Express **13**, 4708 (2005).
[64] R. Osellame, V. Maselli, R. Martinez Vazquez, R. Ramponi, and G. Cerullo, Appl. Phys. Lett. **90**, 231118 (2007).
[65] A. Killi, U. Morgner, M. J. Lederer, and D. Kopf, Opt. Lett. **29**, 1288 (2004).
[66] K. Sugioka, Y. Hanada, and K. Midorikawa, Laser Photonics Rev. **4**, 386 (2010).
[67] Y. Bellouard, A. Said, M. Dugan, and P. Bado, Opt. Express **12**, 2120 (2004).

[68] R. S. Taylor, C. Hnatovsky, E. Simova, D. M. Rayner, M. Mehandale, V. R. Bhardwaj, and P. B. Corkum, Opt. Express **11**, 775 (2003).
[69] Y. Shimotsuma, P. Kazansky, J. Qiu, and K. Hirao, Phys. Rev. Lett. **91**, 247405 (2003).
[70] V. R. Bhardwaj, E. Simova, P. P. Rajeev, C. Hnatovsky, R. S. Taylor, D. M. Rayner, and P. B. Corkum, Phys. Rev. Lett. **96**, 057404 (2006).
[71] P. P. Rajeev, M. Gerstvolf, E. Simova, C. Hnatovsky, R. S. Taylor, D. M. Rayner, and P. B. Corkum, Phys. Rev. Lett. **97**, 253001 (2006).
[72] C. Hnatovsky, R. Taylor, E. Simova, V. Bhardwaj, D. Rayner, and P. B. Corkum, Opt. Lett. **30**, 1867 (2005).
[73] Y. Cheng, K. Sugioka, K. Midorikawa, M. Masuda, K. Toyoda, M. Kawachi, and K. Shihoyama, Opt. Lett. **28**, 55 (2003).
[74] V. Maselli, R. Osellame, G. Cerullo, R. Ramponi, P. Laporta, L. Magagnin, and P. L. Cavallotti, Appl. Phys. Lett. **88**, 191107 (2006).
[75] F. He, H. Xu, Y. Cheng, J. Ni, H. Xiong, Z. Xu, K. Sugioka, and K. Midorikawa, Opt. Lett. **35**, 1106 (2010).
[76] C. Hnatovsky, R. S. Taylor, E. Simova, P. P. Rajeev, D. M. Rayner, V. R. Bhardwaj, and P. B. Corkum, Appl. Phys. A, Mater. Sci. Process. **84**, 47 (2006).
[77] F. Venturini, W. Navarrini, G. Resnati, P. Metrangolo, R. Martinez Vazquez, R. Osellame, and G. Cerullo, J. Phys. Chem. C **114**, 18712 (2010).
[78] K. C. Vishnubhatla, N. Bellini, R. Ramponi, G. Cerullo, and R. Osellame, Opt. Express **17**, 8685 (2009).
[79] S. Kiyama, S. Matsuo, S. Hashimoto, and Y. Morihira, J. Phys. Chem. C **113**, 11560 (2009).
[80] M. Boero, A. Oshiyama, P. L. Silvestrelli, and K. Murakami, Appl. Phys. Lett. **86**, 201910 (2005).
[81] J. P. Landers, Handbook of capillary and microchip electrophoresis and associated microtechniques (CRC Press, New York, 2008)
[82] J. P. Landers, Anal. Chem. **75**, 2919 (2003).
[83] S. Ghosal, Electrophoresis **25**, 214 (2004).
[84] R. Martinez Vazquez, R. Osellame, D. Nolli, C. Dongre, H. van den Vlekkert, R. Ramponi, M. Pollnau, and G. Cerullo, Lab Chip **9**, 91 (2009).
[85] C. Dongre, R. Dekker, H. J. W. M. Hoekstra, M. Pollnau, R. Martinez-Vazquez, R. Osellame, G. Cerullo, R. Ramponi, R. van Weeghel, G. A. J. Besselink, and H. H. van den Vlekkert, Opt. Lett. **33**, 2503 (2008).
[86] R. Martinez Vazquez, R. Osellame, M. Cretich, M. Chiari, C. Dongre, H. J. W. M. Hoekstra, M. Pollnau, H. van den Vlekkert, R. Ramponi, and G. Cerullo, Anal. Bioanal. Chem. **393**, 1209 (2009).
[87] C. Dongre, J. van Weerd, R. van Weeghel, R. Martinez Vazquez, R. Osellame, G. Cerullo, M. Cretich, M. Chiari, H. J. W. M. Hoekstra, and M. Pollnau, Electrophoresis **31**, 2584 (2010).
[88] M. Cretich, M. Chiari, G. Pirri, and A. Crippa, Electrophoresis **26**, 1913 (2005).
[89] H. Tian and J. P. Landers, Anal. Biochem. **309**, 212 (2002).
[90] C. L. Bliss, J. N. McMullin, and C. J. Backhouse, Lab Chip **7**, 1280 (2007).
[91] B. M. Paegel, C. A. Emrich, G. J. Wedemeyer, J. R. Scherer, and R. A. Mathies, Proc. Natl. Acad. Sci. USA **99**, 574 (2002).
[92] C. Dongre, J. van Weerd, N. Bellini, R. Osellame, and G. Cerullo, R. van Weeghel, H. J. W. M. Hoekstra, and M. Pollnau, Biomed. Opt. Express **1**, 729 (2010).
[93] H. T. Li, L. M. Ying, J. J. Green, S. Balasubramanian, and D. Klenerman, Anal. Chem. **75**, 1664 (2003).
[94] P. Dumais, C. L. Callender, J. P. Noad, and C. J. Ledderhof, IEEE Sensors J. **8**, 457 (2008).
[95] R. G. Heideman and P. V. Lambeck, Sens. Actuators B Chem. **61**, 100 (1999).
[96] A. Ymeti, J. Greve, P. V. Lambeck, T. Wink, S. W. F. M. v. Hovell , T. A. M. Beumer, R. R. Wijn, R. G. Heideman, V. Subramaniam, and J. S. Kanger, Nano Lett. **7**, 394 (2007).
[97] A. S. Jugessur, J. Dou, J. S. Aitchison, R. M. De La Rue, and M. Gnan, Microelectron. Eng. **86**, 1488 (2009).
[98] D. Yin, E. J. Lunt, M. I. Rudenko, D. W. Deamer, A. R. Hawkins, and H. Schmidt, Lab Chip **7**, 1171 (2007).
[99] S. J. Haswell, R. J. Middleton, B. O'Sullivan, V. Skelton, P. Watts, and P. Styring, Chem. Commun. **5**, 391 (2001).
[100] A. Crespi, Yu Gu, H. J. W. M. Hoekstra, C. Dongre, M. Pollnau, R. Ramponi, G. Cerullo, and R. Osellame, Lab Chip **10**, 1167 (2010).
[101] V. Maselli, J. R. Grenier, S. Ho, and P. R. Herman, Opt. Express **17**, 11719 (2009).
[102] H. Zhang, S. M. Eaton, and P. R. Herman, Opt. Lett. **32**, 2559 (2007).
[103] R. W. Applegate, Jr., J. Squier, T. Vested, J. Oakey, D. W. M. Marr, P. Bado, M. A. Dugan, and A. A. Said, Lab Chip **6**, 422 (2006).
[104] M. Kim, D. J. Hwang, H. Jeon, K. Hiromatsu, and C. P. Grigoropoulos, Lab Chip **9**, 311 (2009).
[105] D. J. Hwang, M. Kim, K. Hiromatsu, H. Jeon, and C. P. Grigoropoulos, Appl. Phys. A **96**, 385 (2009).
[106] Z. Wang, J. El-Ali, M. Engelund, T. Gotsaed, I. R. Perch-Nielsen, K. B. Mogensen, D. Snakenborg, J. P. Kutter, and A. Wolff, Lab Chip **4**, 372 (2004).
[107] L. M. Fu, R. J. Yang, C. H. Lin, Y. J. Pan, and G. B. Lee, Anal. Chim. Acta **507**, 163 (2004).
[108] D. G. Grier, Nature **424**, 810 (2003).
[109] J. E. Molloy and M. J. Padgett, Contemp. Phys. **43**, 241 (2002).
[110] C. Liberale, P. Minzioni, F. Bragheri, F. De Angelis, E. Di Fabrizio, and I. Cristiani, Nature Photon. **1**, 723 (2007).
[111] J. Guck, S. Schinkinger, B. Lincoln, F. Wottawah, S. Ebert, M. Romeyke, D. Lenz, H. M. Erickson, R. Ananthakrishnan, D. Mitchell, J. Käs, S. Ulvick, and C. Bilby, Biophys. J. **88**, 3689 (2005).
[112] J. Guck, R. Ananthakrishnan, H. Mahmood, T. J. Moon, C. C. Cunningham, and J. Käs, Biophys. J. **81**, 767 (2001).
[113] A. Ashkin, Phys. Rev. Lett. **24**, 156 (1970).
[114] A. Constable, J. Kim, J. Mervis, F. Zarinetchi, and M. Prentiss, Opt. Lett. **18**, 1867 (1993).
[115] B. Lincoln, S. Schinkinger, K. Travis, F. Wottawah, S. Ebert, F. Sauer, and J. Guck, Biomed. Microdevices **9**, 703 (2007).
[116] N. Bellini, K. C. Vishnubhatla, F. Bragheri, L. Ferrara, P. Minzioni, R. Ramponi, I. Cristiani, and R. Osellame, Opt. Express **18**, 4679 (2010).
[117] F. Bragheri, L. Ferrara, N. Bellini, K. C. Vishnubhatla, P. Minzioni, R. Ramponi, R. Osellame, and I. Cristiani, J. Biophoton. **3**, 234 (2010).